Semaphorin 3A overcomes cancer hypoxia and metastatic dissemination induced by antiangiogenic treatment in mice

Federica Maione,[1,2,3] Stefania Capano,[1,2,3] Donatella Regano,[1,2,3] Lorena Zentilin,[4] Mauro Giacca,[4] Oriol Casanovas,[5] Federico Bussolino,[2,3,6,7] Guido Serini,[2,3,7,8] and Enrico Giraudo[1,2,3,7]

[1]Laboratory of Transgenic Mouse Models, [2]IRCC, and [3]Department of Oncological Sciences, University of Torino School of Medicine, Candiolo, Italy. [4]International Centre for Genetic Engineering and Biotechnology (ICGEB), Molecular Medicine Laboratory, Trieste, Italy. [5]Tumor Angiogenesis Group, Translational Research Laboratory, Catalan Institute of Oncology — IDIBELL, L'Hospitalet de Llobregat, Spain. [6]Laboratory of Vascular Oncology, University of Torino School of Medicine, Candiolo, Italy. [7]Center for Complex Systems in Molecular Biology and Medicine (SysBioM), University of Torino, Torino, Italy. [8]Laboratory of Cell Adhesion Dynamics, University of Torino School of Medicine, Candiolo, Italy.

Cancer development, progression, and metastasis are highly dependent on angiogenesis. The use of antiangiogenic drugs has been proposed as a novel strategy to interfere with tumor growth, but cancer cells respond by developing strategies to escape these treatments. In particular, animal models show that antiangiogenic drugs currently used in clinical settings reduce tumor tissue oxygenation and trigger molecular events that foster cancer resistance to therapy. Here, we show that semaphorin 3A (Sema3A) expression overcomes the proinvasive and prometastatic resistance observed upon angiogenesis reduction by the small-molecule tyrosine inhibitor sunitinib in both pancreatic neuroendocrine tumors (PNETs) in RIP-Tag2 mice and cervical carcinomas in HPV16/E_2 mice. By improving cancer tissue oxygenation and extending the normalization window, Sema3A counteracted sunitinib-induced activation of HIF-1α, Met tyrosine kinase receptor, epithelial-mesenchymal transition (EMT), and other hypoxia-dependent signaling pathways. Sema3A also reduced tumor hypoxia and halted cancer dissemination induced by DC101, a specific inhibitor of the VEGF pathway. As a result, reexpressing Sema3A in cancer cells converts metastatic PNETs and cervical carcinomas into benign lesions. We therefore suggest that this strategy could be developed to safely harnesses the therapeutic potential of the antiangiogenic treatment.

Introduction

Angiogenesis is required for invasive tumor growth and metastatic dissemination, providing the rationale for the development of antiangiogenic therapies (1). Despite the generation of innovative antiangiogenic strategies, such as inhibitors of the VEGF-A pathway, resistance to anti-VEGF therapy has been recently observed in both preclinical and clinical trials (2, 3). For instance, preclinical studies provided evidence for anti-VEGF drug evasion by activation of alternate proangiogenic pathways, likely induced by a significant increase of tumor tissue hypoxia (4). Therefore, to extend the optimal therapeutic windows and design more effective antiangiogenic combinatory regimens that could prevent or block tumor invasion and metastasis formation, it is critical to identify new angiogenic modulators and uncover their molecular and cellular mechanisms of action in vivo.

It is well documented that, as a result of architectural and biological abnormalities such as tortuosity, leakiness, and lack of pericytes, tumor blood vessels are structurally and functionally aberrant (5), causing cancer tissue hypoxia (6). Notably, abnormal vascular permeability and chronic oxygen shortage promote tumor invasiveness, for example, by upregulating HIF-1α expression (3, 7), downregulating E-cadherin expression (8), and hyperactivating hepatocyte growth factor/Met (HGF/Met) signaling (9). Furthermore, several independent preclinical studies (10, 11), which have not yet been paralleled by analogous clinical trials, revealed that although impairing cancer angiogenesis with different therapeutic approaches initially causes remarkable shrinkage of the tumor mass, this approach eventually causes dramatic enhancement of tumor invasiveness and increased distal metastasis formation. These data, together with the formal demonstration that improving oxygenation can suppress metastatization of cancer cells and promote their differentiation (12), further support the hypothesis that vascular normalization could represent a remarkably advantageous anticancer strategy, as it is also able to favor chemotherapy delivery and response to radiotherapy (6). We previously showed that endothelial semaphorin 3A (Sema3A) is an endogenous antiangiogenic agent that, when reexpressed in cancers that lost it, is able to normalize the vasculature and to block tumor growth, finally inducing a stable disease (13). In the present study, we investigated the molecular and cellular mechanisms by which Sema3A, alone or in combination with different antiangiogenic drugs, is able to impair tumor cell dissemination and overcome evasive resistance to angiogenesis inhibition (14).

Results

Sema3A halts tumor invasion and metastasis formation caused by antiangiogenic treatment. We previously demonstrated that reexpressing Sema3A in tumors of a spontaneous mouse model of pancreatic neuroendocrine cancer (RIP-Tag2) by somatic gene transfer using adeno-associated virus–8 (AAV8) resulted in reduced vascular density, inhibition of tumor growth, significant survival extension, normalization of tumor vasculature, and decreased tumor hypoxia (13). Stemming from these data, we sought to investigate whether

Conflict of interest: The authors have declared that no conflict of interest exists.
Citation for this article: *J Clin Invest.* 2012;122(5):1832–1848. doi:10.1172/JCI58976.

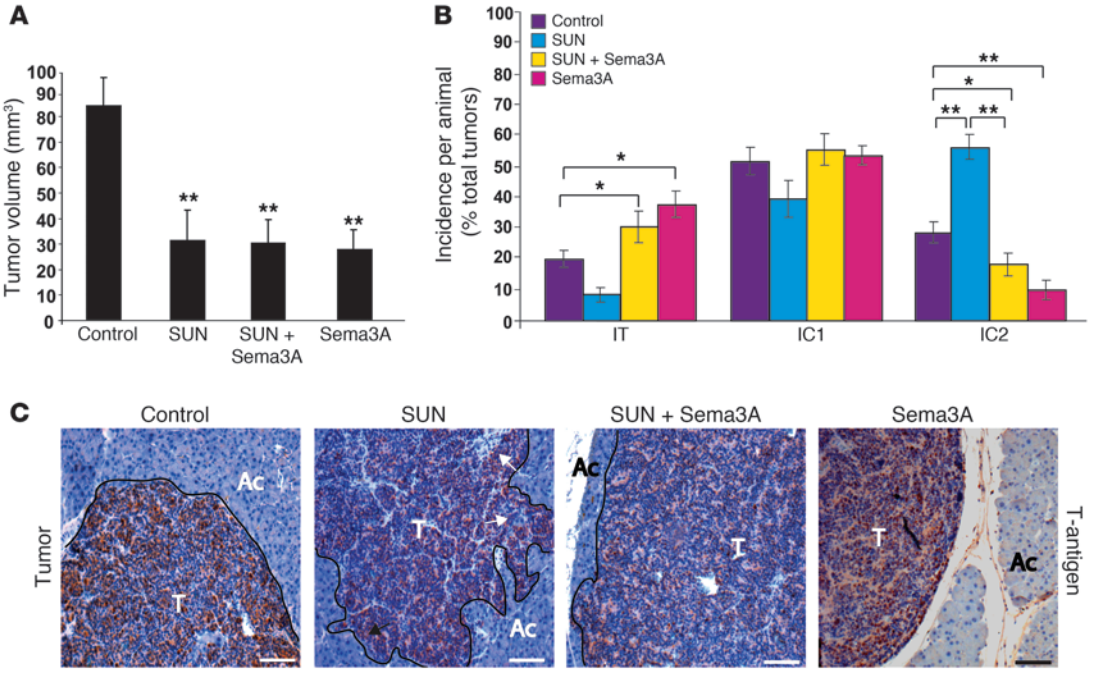

Figure 1
Sema3A blocks tumor invasion caused by antiangiogenic treatment. (**A**) Total tumor volume in 4-week treatment regression trial (from 12 to 16 weeks of age) showed that sunitinib (SUN), AAV8-Sema3A in combination with sunitinib, and AAV8-Sema3A reduced tumor burden 64%, 63%, and 66%, respectively, compared with controls (AAV8-LacZ–injected RIP-Tag2 treated with vehicle; see Methods). (**B**) Percent encapsulated (IT), microinvasive (IC1), and fully invasive (IC2) carcinomas. Combined AAV8-Sema3A and sunitinib decreased IC2 carcinoma incidence 62% compared with sunitinib alone. Sema3A-treated tumors showed a statistically significant 64% decrease of IC2 carcinomas compared with controls. (**C**) Analysis of tumor invasiveness by means of SV40 T-antigen immunostaining. Sunitinib-treated tumors displayed an invasive front extensively intercalated into the surrounding tissue (arrows). T, tumor; Ac, acinar tissue. *$P < 0.05$, **$P < 0.01$, unpaired Mann-Whitney *U* test. Scale bars: 50 μm.

Sema3A also impairs tumor invasion and metastasis formation to overcome the evasive resistance observed in RIP-Tag2 mice and other mouse models in response to antiangiogenic therapies (10, 11). We first compared the effect of AAV8-Sema3A (referred to herein as Sema3A) and sunitinib, a prototypical small-molecule tyrosine kinase (TK) inhibitor and antiangiogenic drug (15), on tumor dissemination in RIP-Tag2 mice by performing a 4-week regression trial between 12 and 16 weeks of age. Treatment of tumor-bearing RIP-Tag2 mice with sunitinib induced primary tumor shrinkage and strongly inhibited angiogenesis (see below), but at the same time promoted local invasiveness and distant metastasis formation compared with controls (Figure 1, Figure 2, A–G, and Supplemental Figure 1; supplemental material available online with this article; doi:10.1172/JCI58976DS1), consistent with previous findings (10). On the contrary, treatment with Sema3A alone not only reduced tumor burden and vascularization (ref. 13 and see below), but also dramatically decreased cancer invasion in the surrounding tissues as well as the incidence and volume of peripancreatic LN metastases and the incidence, number, and volume of liver metastases compared with controls (Figure 1 and Figure 2, A–G). Hence, we showed Sema3A to be an angiogenesis inhibitor that, differently from sunitinib, also displayed a powerful antimetastatic activity. The recent observation that systemic delivery of Sema3A inhibits angiogenesis and metastatization in xenograft tumor models as well (16) further supports the role of Sema3A as an effective pharmacological inhibitor of cancer progression. To start investigating whether Sema3A antagonizes the previously described proinvasive effect of sunitinib in RIP-Tag2 mice (10), we set up a combinatory therapeutic regimen, treating RIP-Tag2 mice simultaneously with Sema3A and sunitinib for 1 month, after which we assessed the frequency of invasive lesions and metastasis formation. Notably, the combination of Sema3A with sunitinib strongly reduced the incidence of fully invasive (IC2) tumors and the extent of both LN and liver metastases in sunitinib-treated animals (Figure 1, B and C, and Figure 2, A–G). Together, these data demonstrated that Sema3A not only impaired metastasis formation during spontaneous tumorigenesis, but also curbed the increased cancer aggressiveness stimulated by sunitinib treatment.

Sema3A and sunitinib synergize to enhance survival. Based on our observation that the combination of Sema3A with sunitinib effectively hampered the evasive resistance elicited by sunitinib treatment alone in RIP-Tag2 mice, we next investigated whether these 2 drugs could synergistically impair tumor progression and hence extend RIP-Tag2 survival as well. We performed a longer survival trial in which RIP-Tag2 tumor-bearing mice were treated beginning at 12 weeks of age with AAV8-LacZ (referred to herein as LacZ) plus vehicle (control), Sema3A, sunitinib, or combined Sema3A and sunitinib. The median survival of control mice was 2.5 weeks. Similar to our previous observations (13), Sema3A significantly prolonged the survival of RIP-Tag2 mice by 9.0 weeks compared with control-treated animals ($P < 0.001$), 2.3 weeks longer than that observed with sunitinib treatment alone ($P < 0.01$). Treatment

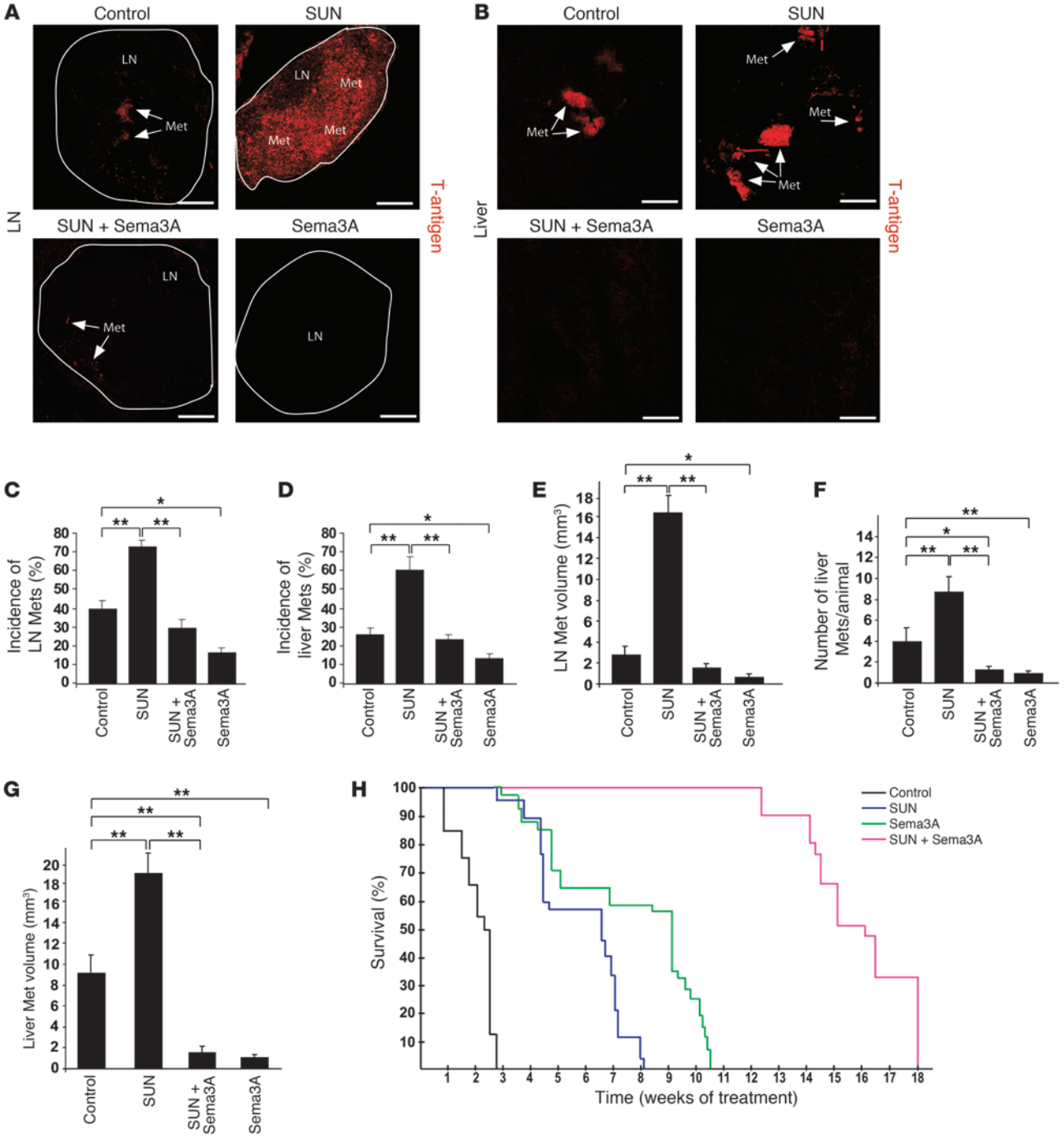

Figure 2

Sema3A blocks distal metastasis formation caused by antiangiogenic treatment. (**A** and **B**) SV40 T-antigen immunostaining (arrows) of peripancreatic LN and liver metastases (Met). Representative images were derived from serial section analysis in each animal (n = 30 per treatment group). (**C** and **D**) Metastasis incidence per animal. Combined Sema3A and sunitinib decreased LN and liver metastases 57% and 54%, respectively, compared with sunitinib alone. Sema3A reduced LN and liver metastases 62% and 50%, respectively, compared with controls. (**E**) LN metastasis volume. Combined Sema3A and sunitinib decreased LN volume 89% compared with sunitinib alone; Sema3A decreased LN volume 79% compared with controls. (**F** and **G**) Number (**F**) and volume (**G**) of liver metastases (n = 30 per treatment group). Combined Sema3A and sunitinib diminished the number and volume of liver metastases 88% and 91%, respectively, compared with sunitinib alone; Sema3A reduced liver metastasis number and volume 80% and 85%, respectively, compared with controls. (**H**) Survival trial in tumor-bearing RIP-Tag2 mice treated continuously with 40 mg/kg/d sunitinib, Sema3A, combined Sema3A and sunitinib, or LacZ beginning at 12 weeks (n = 20 per group). *P < 0.05, **P < 0.01, unpaired Mann-Whitney U test or log-rank test (for survival trials). Scale bars: 50 μm.

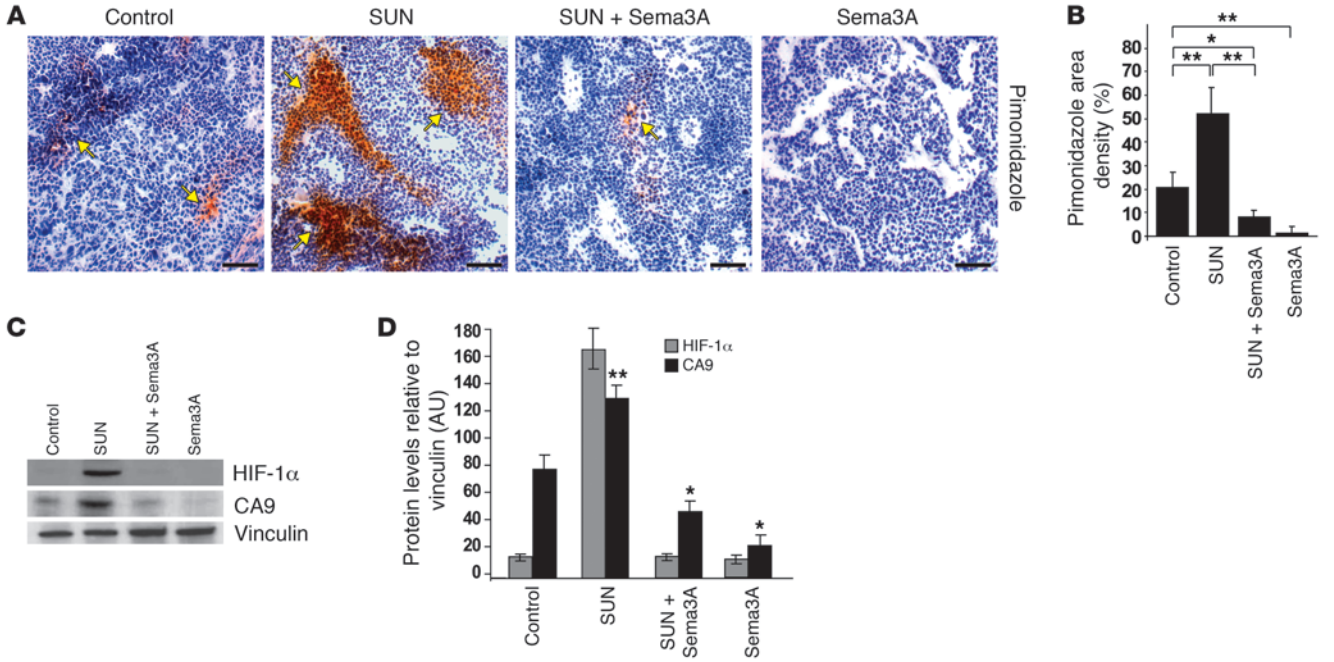

Figure 3

Sema3A impairs basal and sunitinib-elicited tumor hypoxia and HIF-1α expression. (**A**) Tumor hypoxia was assessed by means of pimonidazole adduct immunostaining (arrows) in serial sections of tumors of RIP-Tag2 mice treated for 4 weeks with sunitinib, Sema3A, and the combination compared with control. Representative images were derived from serial section analysis in each animal (n = 15 per treatment group). (**B**) Quantification of hypoxic tumors, expressed as percent of pimonidazole density area per tumor, per animal. Combined Sema3A and sunitinib reduced hypoxic area 84% compared with sunitinib alone; Sema3A decreased hypoxic area 90% compared with controls. (**C**) Western blot analysis of HIF-1α, CA9, and vinculin (as protein loading control) in tumors isolated from RIP-Tag2 mice treated as indicated. (**D**) Relative levels of HIF-1α and CA9 protein expression, normalized to vinculin (n = 12 per treatment group). Combined Sema3A and sunitinib diminished HIF-1α expression and CA9 amount 91% and 60%, respectively, compared with sunitinib alone; Sema3A decreased CA9 expression 55% compared with control. *P < 0.05, **P < 0.01, unpaired Mann-Whitney U test. Scale bars: 50 μm.

with sunitinib increased survival 6.7 weeks compared with controls (P < 0.001) (Figure 2H), as previously shown (10). Interestingly, this survival trial clearly demonstrated that the combination of Sema3A with sunitinib significantly enhanced the survival of RIP-Tag2 mice by 16.2, 7.2, and 9.5 weeks compared with control, Sema3A, and sunitinib, respectively (P < 0.001 for all comparisons; Figure 2H), suggestive of effective synergism of Sema3A and sunitinib regarding survival and tumor progression. Of note, 18 weeks after the initial treatment with combined Sema3A and sunitinib, 6 of 20 mice of the survival trial were still alive, and 2 of these were tumor free. Interestingly, similarly to what we observed in the 4-week regression trial, this combinatorial treatment resulted in very small and round tumors (Supplemental Figure 4A) and strongly halted tumor invasiveness in the RIP-Tag2 mice that survived until the end of the trial. Importantly, none of the 6 surviving mice had liver or peripancreatic LN metastases. Together, these data indicate that the combination of Sema3A with sunitinib results in a synergistic effect by prolonging animal survival and inducing smaller, less invasive, and less frequent metastatic cancers.

Sema3A counteracts basal and sunitinib-elicited tumor hypoxia. Both primary tumors and metastases of mice treated with antiangiogenic drugs are highly hypoxic (10), and preclinical studies suggest that evasion to antiangiogenic therapies could depend on the hypoxia-driven induction of alternative proangiogenic pathways in tumor cells (4, 14). Based on the vascular normalizing effect of Sema3A we previously observed in RIP-Tag2 tumors (13), we hypothesized that this molecule could overcome the evasive resistance to angiogenesis inhibition by hampering tumor hypo-oxygenation. We therefore measured tissue hypoxia in RIP-Tag2 insulinomas treated with sunitinib, Sema3A, or both in combination. The strong reduction of vessel area induced by sunitinib was accompanied by an increase in intratumoral hypoxia, as assessed by pimonidazole staining (Figure 3, A and B). As previously shown, treating RIP-Tag2 mice with Sema3A for 1 month proportionally restrained the amount of blood vessels and normalized the remaining vasculature, abrogating the tumor hypoxia observed in control mice at both the beginning and the end of the therapeutic trial (ref. 13 and Supplemental Figure 2). Remarkably, combinatory treatment with Sema3A completely reversed the sizeable hypoxia observed in sunitinib-treated RIP-Tag2 insulinomas (Figure 3, A and B).

To further characterize the extent of tumor hypoxia associated with the different therapeutic regimens, we assessed the expression of HIF-1α, a master regulator of cellular adaptation to oxygen deprivation that acts as a survival factor for hypoxic cancer cells, being expressed in many human cancers and associated with poor prognosis and treatment failure (3, 7). Remarkably, Western blot analysis revealed a strong increase of HIF-1α protein in sunitinib-treated tumors that was dramatically reduced by simultaneous treatment with Sema3A (Figure 3, C and D). Of note, administering sunitinib, alone or in combination with Sema3A, resulted

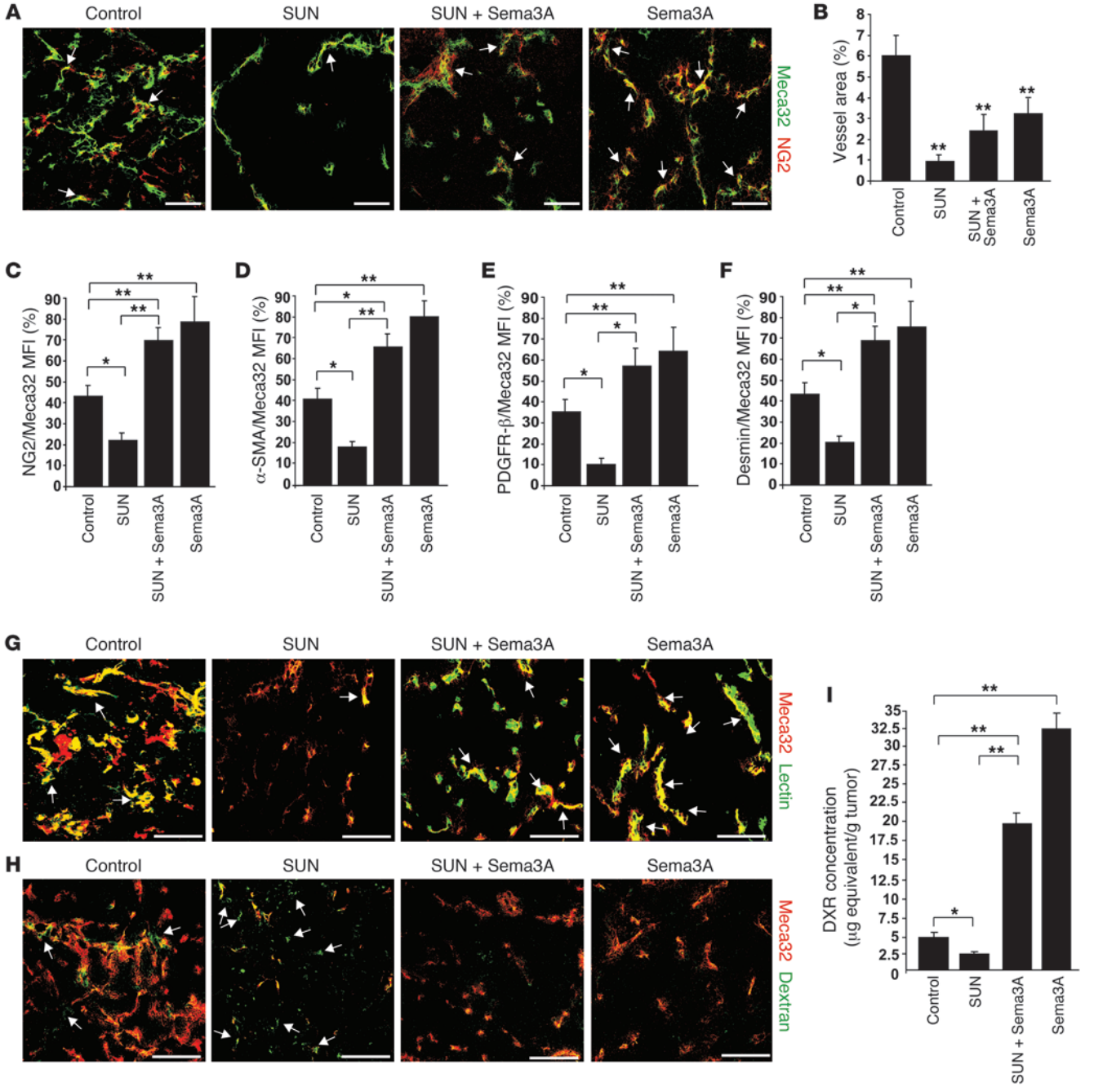

Figure 4

Sema3A alone or in combination with sunitinib enhances pericyte coverage, reduces blood vessel leakage, improves tissue perfusion, and increases doxorubicin delivery to tumors. (**A** and **B**) As assessed by confocal analysis of Meca32 immunostaining, vessel density in RIP-Tag2 tumors after a 4-week regression trial was reduced 89% in sunitinib-treated tumors, 60% in Sema3A and sunitinib–treated tumors, and 47% Sema3A-treated tumors compared with controls. (**A** and **C**–**F**) Pericyte coverage, as evaluated by confocal colocalization analysis of Meca32 with NG2 (**A**, arrows, and **C**) or with α-SMA (**D**), PDGFR-β (**E**), or desmin (**F**). Combined Sema3A and sunitinib enhanced pericyte coverage 62% (NG2), 72% (α-SMA), 84% (PDGFR-β), and 69% (desmin) compared with sunitinib alone; Sema3A increased pericyte coverage 45% (NG2), 47% (α-SMA), 40% (PDGFR-β), and 43% (desmin) compared with controls. (**G**) In tumors treated with Sema3A alone or in combination with sunitinib, FITC-lectin perfused vessels (arrows) were increased compared with sunitinib-treated and control insulinomas. (**H**) FITC-dextran extravasation (arrows) decreased in tumors treated with Sema3A alone or in combination with sunitinib compared with sunitinib-treated and control insulinomas. Results are from 5 fields per mouse ($n = 12$ per treatment group). (**I**) Amount of doxorubicin (DXR) present in tumors, expressed as μg equivalent/g tumor. Combined Sema3A and sunitinib enhanced doxorubicin 87% compared with sunitinib alone; Sema3A enhanced doxorubicin 83% compared with controls. $^*P < 0.05$, $^{**}P < 0.01$, unpaired Mann-Whitney *U* test. Scale bars: 50 μm.

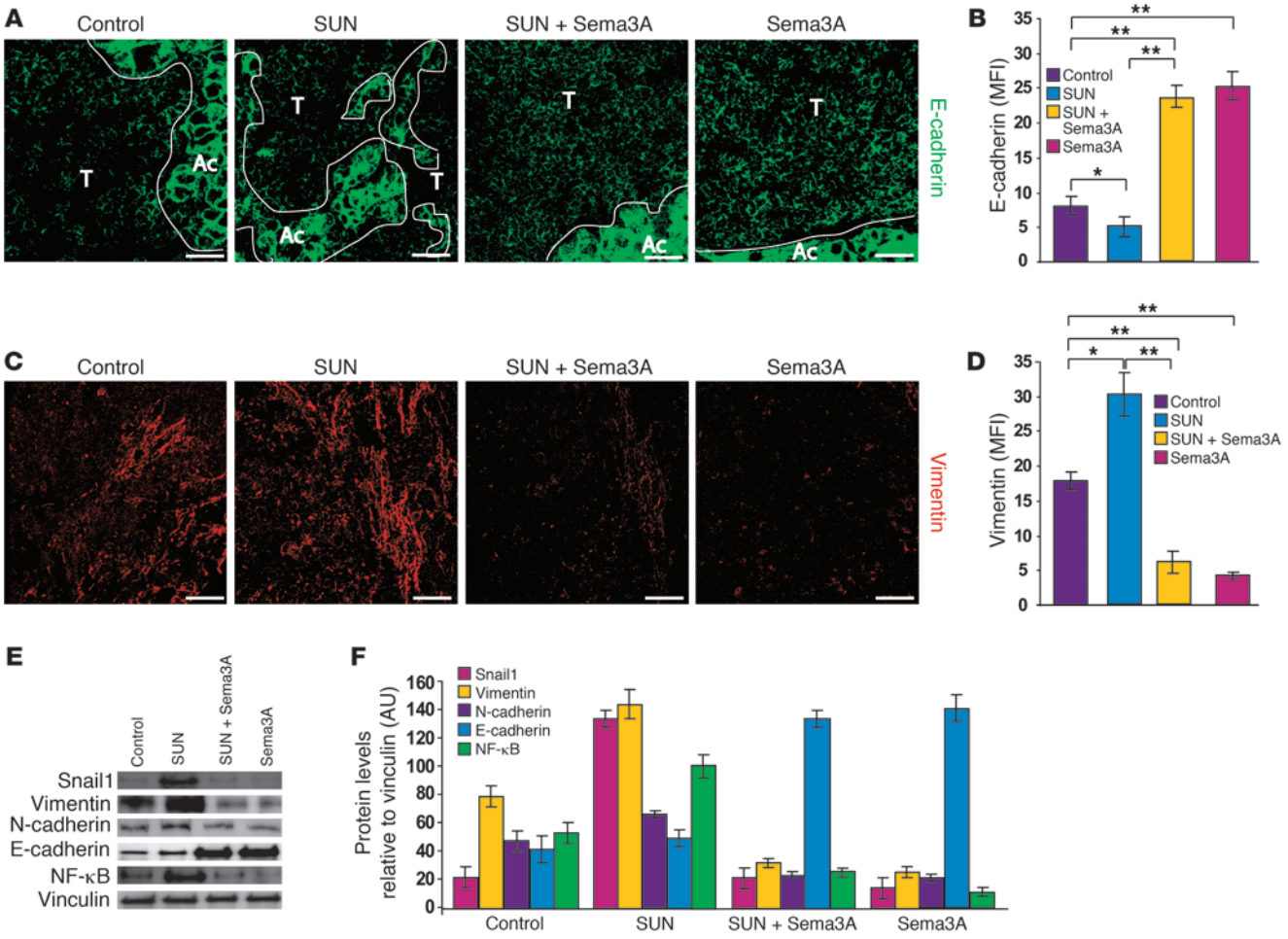

Figure 5

Sema3A reduces both basal and sunitinib-induced EMT and inhibits NF-κB expression. (**A**–**D**) RIP-Tag2 tumors were treated for 4 weeks with sunitinib, AVV8-Sema3A, and the combination; shown are (**A** and **C**) representative confocal microscopy and (**B** and **D**) protein expression, quantified by MFI per animal. (**A** and **B**) Low E-cadherin expression levels in controls and sunitinib-treated insulinomas were significantly upregulated by Sema3A treatment alone or in combination with sunitinib. (**C** and **D**) Increased vimentin expression in sunitinib-treated tumors compared with controls was inhibited by treatment with Sema3A alone or in combination with sunitinib. (**E**) Western blot analysis of protein lysates derived from tumors of the different treatment groups. Sema3A inhibited sunitinib-induced Snail1 and vimentin expression. E-cadherin was highly expressed with Sema3A treatment, alone or in combination with sunitinib, compared with the control and sunitinib alone. Sema3A decreased both basal and sunitinib-induced NF-κB expression. (**F**) Relative protein expression levels of EMT markers and NF-κB expression, normalized to vinculin (n = 6 per treatment group). $^*P < 0.05$, $^{**}P < 0.01$, unpaired Mann-Whitney U test. Scale bars: 50 μm.

in similar modulation of the HIF-1α target gene carbonic anhydrase 9 (CA9) (Figure 3, C and D), which is also upregulated in several human cancers (3, 17). Moreover, in agreement with the normoxic tumor environment induced by Sema3A (ref. 13 and Supplemental Figure 2), we also observed a significant reduction of CA9 in animals treated with Sema3A alone compared with controls (Figure 3, C and D). Thus, by virtue of its ability to normalize tumor blood vessels and to reestablish tissue normoxia, Sema3A efficiently overcame the invasive phenotype elicited by sunitinib in RIP-Tag2 mice.

The combination of Sema3A and sunitinib increases pericyte coverage, reduces blood vessel leakage, enhances tumor tissue perfusion, and prolongs the vascular normalization window. Increased pericyte coverage and reduction in vascular density and branching are hallmarks of tumor blood vessel normalization, a process that occurs in response to some antiangiogenic agents and allows for more efficient delivery of oxygen and chemotherapeutic drugs (6, 18, 19). As expected (10, 15, 20), in sunitinib-treated tumors, in addition to a strong reduction of blood vessel area, we observed remarkable inhibition of pericyte coverage, as revealed by confocal analysis of NG2 staining (Figure 4, A–C). On the contrary, as previously described (13, 20), Sema3A treatment increased the number of perivascular $NG2^+$ cells. Of note, simultaneous treatment with Sema3A and sunitinib significantly increased pericyte coverage (Figure 4, A and C). Similar observations with respect to pericyte coverage in the different treatment groups were obtained using other markers, such as α-SMA, PDGFR-β, and desmin (Figure 4, D–F). To better characterize Sema3A-elicited tumor blood vessel normalization, we further studied the perfusion and permeability of the tumor vasculature of RIP-Tag2 mice undergoing different therapeutic

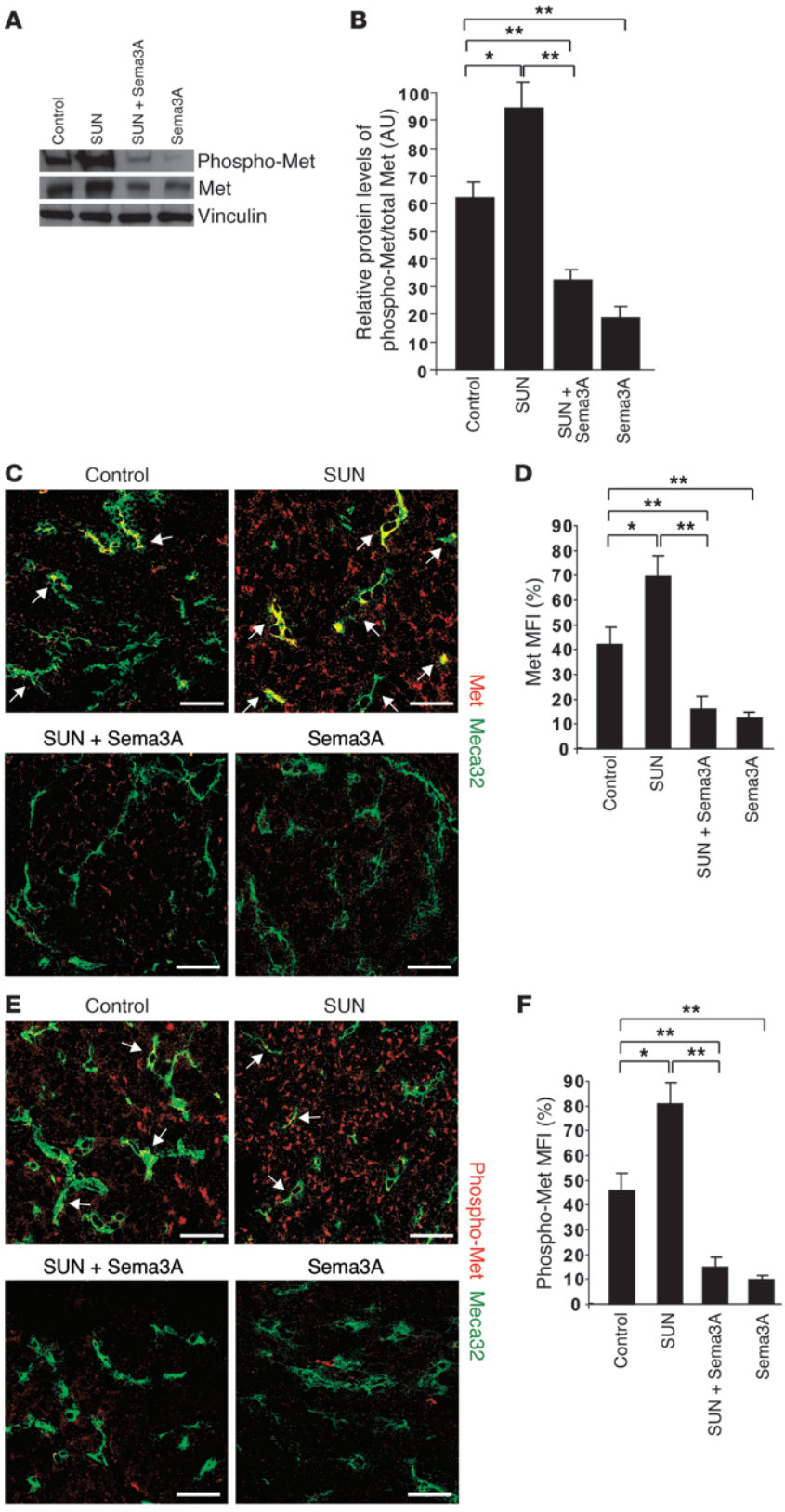

Figure 6
Sema3A inhibits basal and sunitinib-induced expression and activation of Met TK receptor. (**A**) Protein analysis showed greater total Met and phospho-Met in RIP-Tag2 tumors treated with sunitinib compared with controls; notably, both were reduced by Sema3A, either alone or in combination with sunitinib. Vinculin protein was used as loading control. (**B**) Protein levels of phospho-Met, normalized to total Met. (**C**–**F**) Presence and localization of Met and phospho-Met in RIP-Tag2 tumors treated with sunitinib, Sema3A, and the combination compared with controls, as evaluated by colocalization of anti-Met or anti–phospho-Met Abs with Meca32. Shown are (**C** and **E**) representative confocal microscopy, representative of 5 fields per mouse, and (**D** and **F**) quantification by MFI (n = 8 per treatment group). (**C** and **D**) Total Met was present in a subset of tumor blood vessels and in cancer cells in basal conditions and was highly expressed in both vessels and tumor cells after sunitinib treatment (arrows); combined Sema3A and sunitinib reduced Met both in vessels and tumor cells. (**E** and **F**) Phospho-Met was present in some tumor vessels (arrows) and in cancer cells in basal conditions, but increased mainly in tumor cells in sunitinib-treated animals. Notably, Sema3A alone or combined with sunitinib inhibited both total and phospho-Met. *P < 0.05, **P < 0.01, unpaired Mann-Whitney U test. Scale bars: 50 μm.

regimens. At the end of each scheme of treatment, blood vessel perfusion and permeability were respectively assessed by tail-injecting animals with FITC-lectin and 70-kDa FITC-dextran. Interestingly, Sema3A (both alone and in combination with sunitinib) strongly increased the amount of FITC-lectin in the vasculature of insulinomas (Figure 4G and Supplemental Figure 3, A and C), demonstrating a clear improvement of tumor blood vessel perfusion. Moreover, the therapy with Sema3A significantly reduced both basal and sunitinib-elicited leakiness of tumor blood vessels, as measured by confocal analysis of 70-kDa FITC-dextran extravasation (Figure 4H and Supplemental Figure 3, B and D).

To assess whether Sema3A, alone or in combination with sunitinib, increases the efficacy of tumor blood vessels in delivering a chemotherapeutic drug, we injected doxorubicin in RIP-Tag2 mice that were previously treated for 4 weeks with LacZ plus vehicle (control) or with Sema3A, sunitinib, or both in combination, then assessed the amount of drug present within tumor tissues. We detected decreased levels of doxorubicin in insulinomas of sunitinib-treated mice compared with controls (Figure 4I). In contrast,

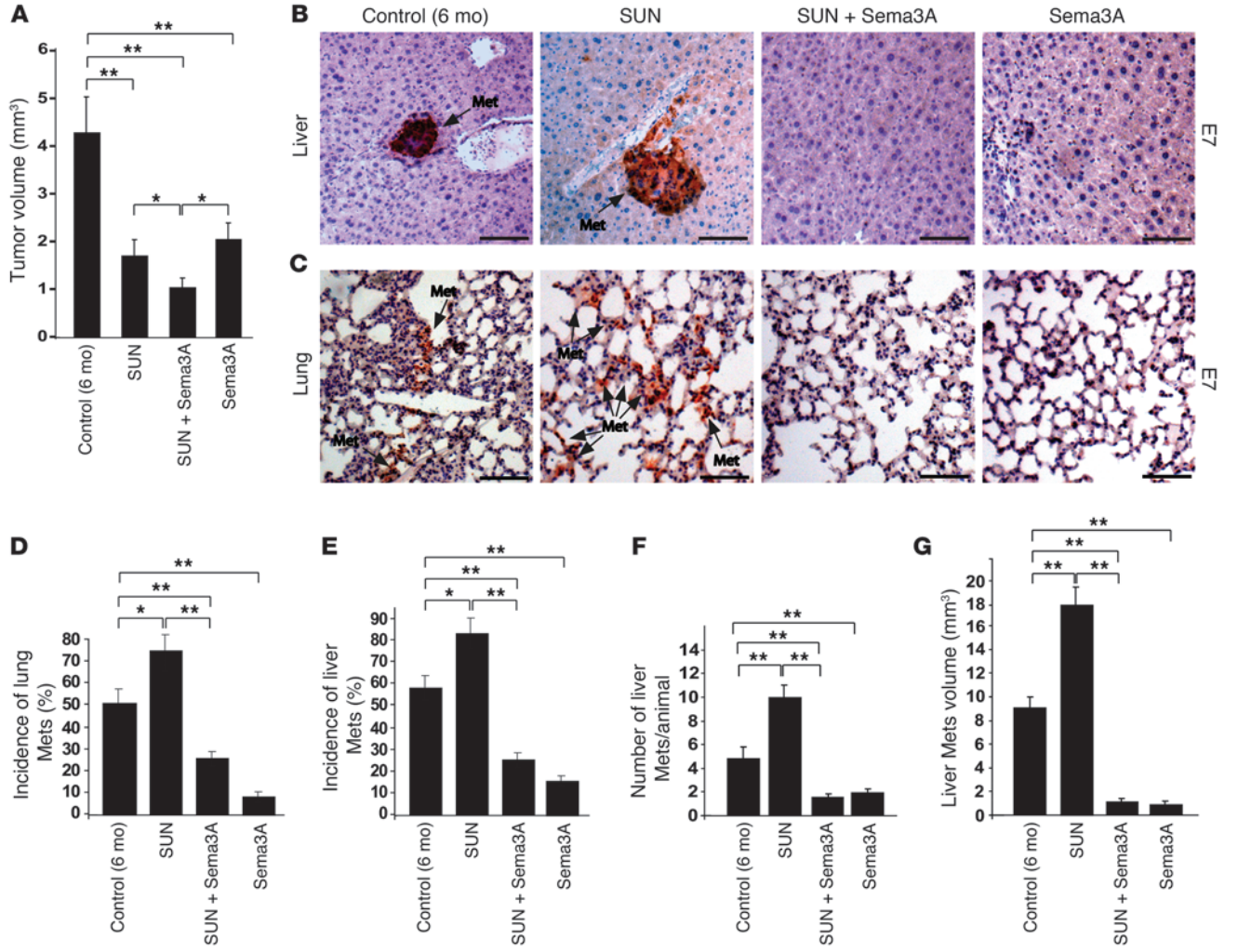

Figure 7

Sema3A halts sunitinib-elicited tumor invasion and metastasis formation in HPV16/E_2 mice. (**A**) Total tumor volume of HPV16/E_2 mice in a 4-week regression trial (from 5 to 6 months of age) revealed that sunitinib, Sema3A combined with sunitinib, and Sema3A alone reduced tumor burden 58%, 76%, and 53%, respectively, compared with LacZ-injected, vehicle-treated HPV16/E_2 controls. (**B** and **C**) Liver and lung metastases (arrows), as assessed by oncogene E7 immunostaining. (**D** and **E**) Combined Sema3A and sunitinib decreased lung (**D**) and liver (**E**) metastasis incidence 67% and 70%, respectively, compared with sunitinib; Sema3A reduced lung and liver metastasis incidence 84% and 74%, respectively, compared with controls. (**F** and **G**) Combined Sema3A and sunitinib diminished the number (**F**) and volume (**G**) of liver metastases 82% and 94%, respectively, compared with sunitinib; Sema3A reduced liver metastasis number and volume 60% and 92%, respectively, compared with controls. Representative images were derived from serial section analysis of each animal (n = 12 per treatment group). *P < 0.05, **P < 0.01, unpaired Mann-Whitney U test. Scale bars: 50 μm.

greater amounts of doxorubicin were present in Sema3A-treated tumors (alone or in combination with sunitinib) compared with control and sunitinib-treated insulinomas (Figure 4I). Based on these findings, we next investigated whether Sema3A is capable of increasing and sustaining the ability of the cancer vasculature to deliver a drug in tumors over a longer period of time, in the hopes of verifying the presence of an extended normalization window. We evaluated the degree of pericyte coverage, tissue hypoxia, and doxorubicin delivery efficiency to tumors of RIP-Tag2 mice treated with combined Sema3A and sunitinib and found to be alive at the end of the survival trial. Remarkably, similarly to what we observed in the 4-week regression trial (Figure 4, A–I), the insulinomas of the surviving mice treated with combined Sema3A and sunitinib were not hypoxic and displayed a functional, nonleaky vasculature, covered by pericytes (Supplemental Figure 4, B–E), that was able to efficiently deliver doxorubicin to tumors (24.6 ± 2.3 μg equivalents/g tumor). Taken together, these data suggest that Sema3A, alone or in combination with sunitinib, substantially extends the normalization window of tumor blood vessel and improves the delivery efficiency of chemotherapeutic drugs to cancers.

Sema3A impairs sunitinib-induced epithelial-mesenchymal transition and NF-κB expression. To better investigate the molecular mechanisms by which Sema3A effectively counteracts the evasive resistance induced by angiogenesis inhibition in RIP-Tag2 mice, we first evaluated the expression of proteins that are involved in epithelial-mesenchymal transition (EMT) and support cancer cell

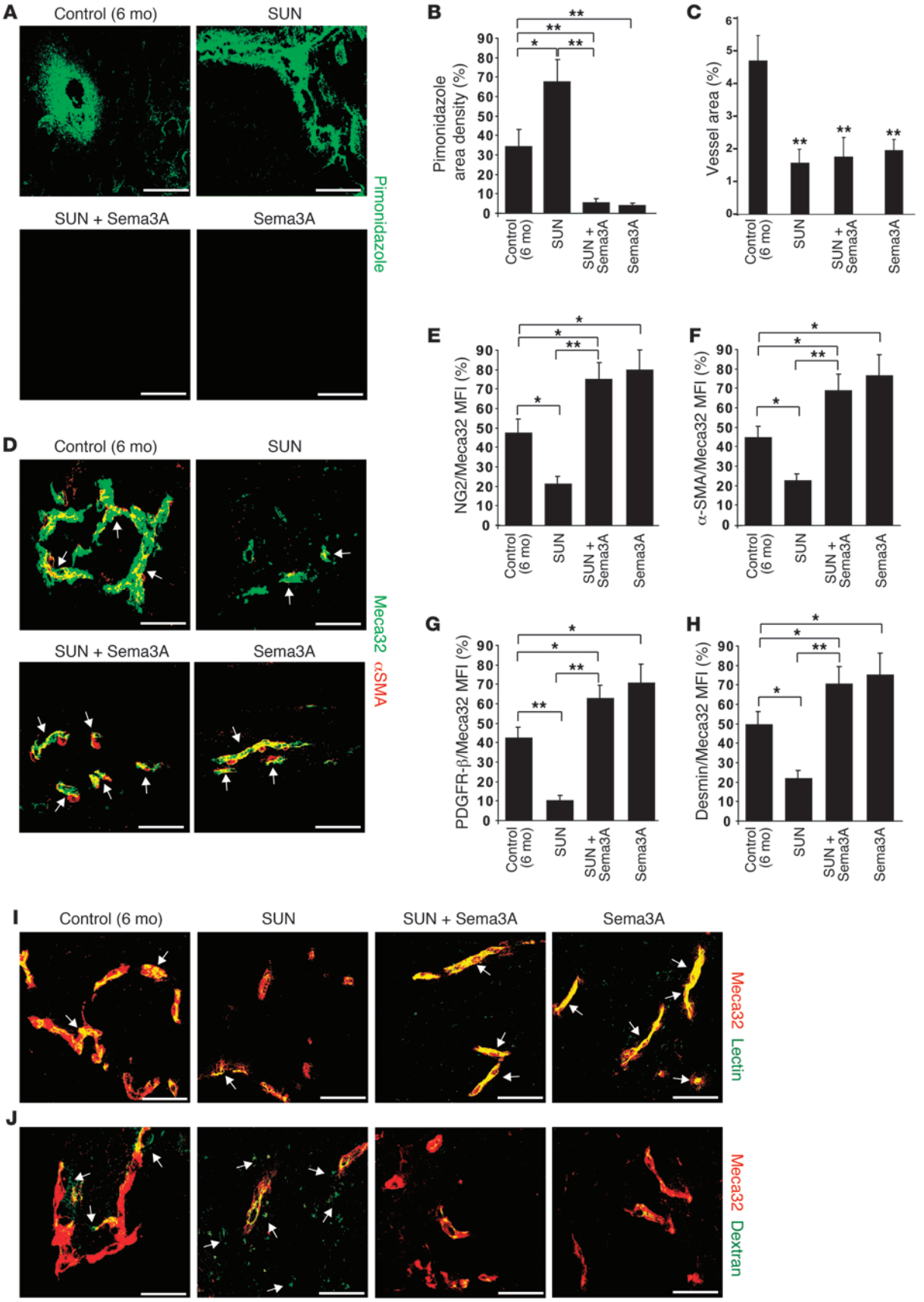
A
Control (6 mo)
SUN
SUN + Sema3A
Sema3A
Pimonidazole
B
Pimonidazole area density (%)
Control (6 mo)
SUN
SUN + Sema3A
Sema3A
C
Vessel area (%)
D
Meca32
αSMA
E
NG2/Meca32 MFI (%)
F
α-SMA/Meca32 MFI (%)
G
PDGFR-β/Meca32 MFI (%)
H
Desmin/Meca32 MFI (%)
I
Meca32
Lectin
J
Meca32
Dextran

Figure 8
Sema3A decreases basal and sunitinib-induced hypoxia in HPV16/E_2 mice by normalizing the tumor vasculature. (**A**) Tumor hypoxia, assessed by pimonidazole adduct immunostaining in serial sections of tumors from HPV16/E_2 mice treated as indicated for 4 weeks. (**B**) Quantification of hypoxic tumors, expressed as percent pimonidazole density area per tumor, per animal. Sema3A and sunitinib combined decreased hypoxia 92% compared with sunitinib alone; Sema3A decreased hypoxia 88% compared with controls. (**C**) Vessel density, as assessed by confocal analysis of Meca32 immunostaining, was reduced 67%, 62%, and 52% by treatment with sunitinib, sunitinib plus Sema3A, and Sema3A, respectively, compared with controls. (**D**–**H**) Pericyte coverage, as evaluated by confocal colocalization (arrows) of Meca32 with α-SMA (**D** and **F**) or with NG2 (**E**), PDGFR-β (**G**), or desmin (**H**) and expressed as percent colocalization of pericyte markers on tumor ECs. Combined Sema3A and sunitinib enhanced pericyte coverage 71% (NG2), 68% (α-SMA), 82% (PDGFR-β), and 69% (desmin) compared with sunitinib alone. Sema3A increased pericyte coverage 40% (NG2), 48% (α-SMA), 39% (PDGFR-β), and 32% (desmin) compared with controls. (**I**) Increased incidence of FITC-lectin–perfused vessels (arrows) in Sema3A-treated (alone or in combination with sunitinib) tumors compared with sunitinib-treated and control insulinomas. (**J**) Decreased FITC-dextran extravasation (arrows) in Sema3A-treated (alone or in combination with sunitinib) tumors compared with sunitinib-treated and control insulinomas. Results are from 5 fields per mouse (n = 8 per treatment group). $^*P < 0.05$, $^{**}P < 0.01$, unpaired Mann-Whitney U test. Scale bars: 50 μm.

metastatic dissemination (21). In EMT, tumor cells typically lose the epithelial marker E-cadherin and gain mesenchymal markers, such as vimentin and N-cadherin (21, 22). In addition, E-cadherin transcriptional repressors, such as Snail1, are also upregulated during EMT (23). Sunitinib-treated tumors demonstrated high expression of Snail1 and the mesenchymal markers vimentin and, to a lesser extent, N-cadherin; in contrast, the Snail1 target E-cadherin was strongly inhibited (Figure 5). Hence, sunitinib treatment promoted invasiveness by activating an EMT program. Remarkably, addition of Sema3A completely reverted the effects of sunitinib, dramatically inhibiting Snail1 and vimentin and enhancing E-cadherin expression (Figure 5). In addition, treating animals with Sema3A alone similarly inhibited the synthesis of mesenchymal markers and promoted E-cadherin expression as well.

NF-κB is involved in both physiological and pathological processes and plays pivotal roles in promoting the EMT-dependent invasive phenotype of several cancers (24, 25). NF-κB induces HIF-1α (26), is activated by hypoxia (27), and is a critical component of the molecular machinery that senses low oxygen levels (28). In agreement with the above data, we observed that NF-κB protein levels were high in tumors treated with sunitinib and that cotreatment with Sema3A returned NF-κB expression levels to those observed with control or Sema3A treatment alone (Figure 5, E and F).

Sema3A inhibits both basal and sunitinib-induced expression and activation of the Met TK receptor. Based on the known inductive effects of hypoxia on the expression and activation of the proinvasive TK receptor Met (9), we assessed total protein and tyrosine phosphorylation levels of Met in treated RIP-Tag2 mice. Western blot analysis revealed that sunitinib treatment caused a significant increase of both total Met and phospho-Met in tumors (Figure 6, A and B). However, whereas total Met immunoreactivity was observed in both blood vessels and tumor cells, phospho-Met was mainly detected in cancer cells (Figure 6, C–F). Interestingly, concomitant Sema3A administration fully inhibited the induction of both total Met and phospho-Met observed with sunitinib treatment alone. Tumors receiving Sema3A alone displayed a similar reduction of Met activation (Figure 6, A–C and E). The clear inhibition of Met TK receptor phosphorylation we observed identified a potential mechanism through which Sema3A might inhibit metastatization, namely the inhibition of Met receptor signaling in tumor cells as result of the reduced tumor hypoxia induced by Sema3A itself.

Sema3A overcomes metastasis formation caused by sunitinib treatment in a mouse model of spontaneous cervical cancer. To evaluate whether the effects of Sema3A on tumor progression during angiogenesis inhibition in RIP-Tag2 mice are recapitulated in another tumor model and histotype, we used the 17β-estradiol–treated K14-HPV16 transgenic mouse model of spontaneous cervical carcinogenesis (referred to herein as HPV16/E_2 mice). In our previous work (13), we identified a similar expression pattern of Sema3A in both HPV16/E_2 and RIP-Tag2 transgenic mouse models; in fact, Sema3A was significantly expressed in normal and angiogenic premalignant stages, but was lost in invasive cervical carcinomas. This cervical cancer model, which recapitulates the progressive development of human cancers, has high and remarkable similarity in terms of both histological and molecular cross-correlation with its corresponding human counterpart (29) and has been widely used to test the effect of antiangiogenic drugs on tumor progression (30).

First, we established an AAV8-based strategy that we believe to be novel to deliver Sema3A in vivo to cervical tumors of HPV16/E_2 mice. To achieve specific gene delivery to the cervix, we established a route of administration by injecting the recombinant AAV8 virus expressing either LacZ (control) or Sema3A-myc in the distal portion of the abdominal aorta, just before its bifurcation into the 2 common iliac arteries. This procedure allowed us to efficiently target and express within the cervix these 2 exogenous gene constructs. We observed that the transformation zone — the area at the border between endo- and ectocervix that undergoes physiological metaplasia, where cervical carcinomas most frequently develop (30, 31) — was efficiently transduced by AAV8 (see Methods and Supplemental Figure 5). This Sema3A delivery strategy allowed us to perform a regression trial with HPV16/E_2 mice, as previously described (30). Tumor-bearing animals were treated with LacZ control or with Sema3A, sunitinib, or the combination for 4 weeks, from the fifth to the sixth month of age. Compared with controls, treatment with either sunitinib or Sema3A alone strongly reduced tumor volume. Interestingly, the combination resulted in much more efficient tumor growth inhibition compared with single drug treatments (Figure 7A).

To assess the effect of the different therapeutic regimens on the formation of distant metastases in HPV16/E_2 mice, we evaluated incidence, volume, and number of micrometastases in vital organs. We evaluated tumor dissemination by means of immunofluorescence and immunohistochemistry using an anti-E7 antibody that specifically detects the HPV16 viral oncogene E7-positive cancer cells in HPV16/E_2 mice organs (Figure 7, B and C). Metastasis incidence in 6-month-old LacZ-treated (control) HPV16/E_2 mouse liver and lungs was 58% and 50%, respectively (Figure 7, D and E). Interestingly, as observed in RIP-Tag2 mice, 1 month of treatment with sunitinib increased liver and lung metastasis incidence to 83% and 75%, respectively. Remarkably, Sema3A, alone and in combination with sunitinib, strongly reduced the percentage of metastases compared with sunitinib- or control-treated mice.

Analysis of metastasis number and volume demonstrated that sunitinib induced a greater number of liver metastases, with

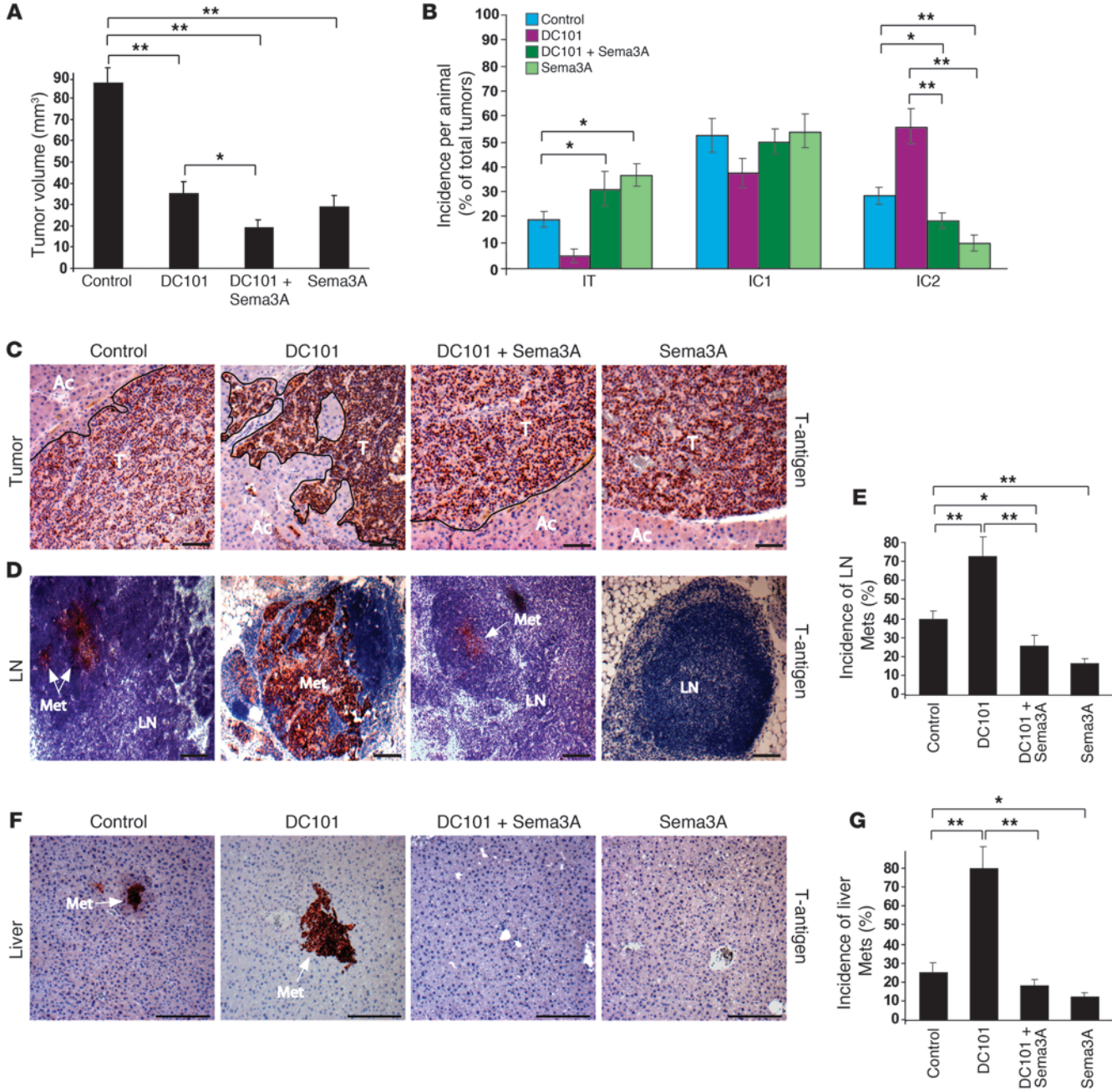

Figure 9

Sema3A blocks DC101-induced cancer invasion and metastatic dissemination. (**A**) Total tumor volume of RIP-Tag2 mice in a 4-week regression trial (from 12 to 16 weeks of age). Treatment with DC101, DC101 plus Sema3A, and Sema3A reduced tumor burden 60%, 79%, and 68%, respectively, compared with LacZ-injected, purified rat IgG–treated RIP-Tag2 controls. (**B**) Percent encapsulated IT, IC1, and IC2 carcinomas. Combined treatment with Sema3A and DC101 decreased IC2 carcinoma incidence 67% compared with DC101 alone. (**C**) DC101-treated tumors displayed highly invasive tumors (arrows), as shown by SV40 T-antigen immunostaining. (**D**–**G**) Analysis of peripancreatic LN (**D** and **E**) and liver (**F** and **G**) metastasis formation. Shown is (**D** and **F**) representative SV40 T-antigen immunostaining, derived from serial sections analysis of each animal, and (**E** and **G**) quantification of metastasis incidence per animal (n = 15 per group). Combined Sema3A and DC101 decreased LN and liver metastasis incidence 64% and 75%, respectively, compared with DC101. Sema3A treatment reduced LN and liver metastasis incidence 62% and 50%, respectively, compared with controls. *P < 0.05, **P < 0.01, unpaired Mann-Whitney U test. Scale bars: 50 μm.

larger volumes, compared with controls (Figure 7, F and G). These data further corroborated the sunitinib-induced evasive resistance previously observed in RIP-Tag2 and other models (10) in a different spontaneous mouse model of carcinogenesis. Notably, Sema3A alone or combined with sunitinib dramatically decreased the degree of liver and lung metastasis formation (Figure 7, B–G). These findings bolster our results obtained with RIP-Tag2 insulinomas, demonstrating that in a very different tumor

type (i.e., cervical cancer), treatment with Sema3A alone hampered tumor invasiveness and dissemination. Moreover, these data strengthen the notion that Sema3A can be conceived as a drug able to overcome the proinvasive and prometastatic effect of sunitinib in different cancer types.

Sema3A reduces basal and sunitinib-induced hypoxia in cervical cancer by normalizing the vasculature. We next sought to determine whether Sema3A counteracts the prometastatic effect of sunitinib in the HPV16/E_2 model by reducing tumor hypoxia, as was observed in RIP-Tag2 mice. We analyzed tumor hypoxia by pimonidazole immunostaining. Control HPV16/E_2 mice displayed a substantial amount of hypoxia both in CIN3 premalignant lesions and in cervical tumors (Figure 8, A and B). As observed in RIP-Tag2 mice, treating HPV16/E_2 mice with sunitinib significantly enhanced hypoxic levels in tumors, in CIN3 lesions, and in the transformation zone (Figure 8A). Sema3A, alone and in combination with sunitinib, strongly reduced both basal and sunitinib-induced tumor hypoxia (Figure 8, A and B). Interestingly, the increase in tissue hypoxia is a critical factor that promotes cervical carcinogenesis and has been associated with shorter progression-free and overall survival and with treatment failure in clinic (32). Therefore, the reduced hypoxia may represent a major mechanism by which Sema3A reduces cervical cancer progression and the metastatic spreading induced by sunitinib.

To confirm that Sema3A decreases tumor hypoxia by promoting blood vessel normalization in the HPV16/E_2 model, we characterized pericyte coverage of tumor blood vessels by confocal microscopy analysis of the pericyte markers NG2, α-SMA, PDGFR-β, and desmin. Similar to our findings in RIP-Tag2 mice (Figure 4, A–F), we observed that 1 month of sunitinib treatment in tumor-bearing HPV16/E_2 mice significantly decreased blood vessel area and greatly reduced pericyte coverage compared with controls (Figure 8, C–H). As expected, Sema3A lessened blood vessel area, but at the same time induced blood vessel normalization by reducing vascular branching and increasing the extent of pericyte coverage of the vasculature compared with sunitinib or control treatments. Notably, combined Sema3A and sunitinib treatment restored pericyte coverage compared with sunitinib alone and induced a vascular phenotype similar to that observed in tumors treated with Sema3A alone. Next, we assessed blood vessel perfusion and permeability in order to determine the functionality of the tumor vasculature. In line with the pericyte coverage analysis, we found very poorly perfused and highly permeable blood vessels in sunitinib-treated carcinomas, whereas treatment with Sema3A (alone or in combination with sunitinib) promoted the formation of a highly perfused and less leaky tumor vasculature (Figure 8, I and J, and Supplemental Figure 6, A–D). Together, these data in a transgenic mouse model of cancer other than RIP-Tag2 compellingly suggest that, by normalizing tumor vasculature and consequently reducing hypoxia, Sema3A is capable of halting cancer invasiveness and metastatic spreading while inhibiting tumor angiogenesis.

Sema3A overcomes the evasive resistance induced by an inhibitor of the VEGF pathway. In order to evaluate whether Sema3A is able to overcome the resistance to antiangiogenic therapies that specifically and selectively interfere with the VEGF signaling pathway, we used DC101, a function-blocking rat monoclonal antibody raised against VEGFR-2 and previously used in the RIP-Tag2 mouse model to assess the evasive resistance to angiogenesis inhibition (4, 10). Similar to the trials performed with sunitinib, we treated RIP-Tag2 mice for 4 weeks with DC101 alone or in combination with Sema3A and compared them with mice treated with Sema3A alone or LacZ plus purified IgG control. Treatment with DC101 exerted effects similar to those we obtained with sunitinib in RIP-Tag2 mice as well as previously described findings (10). Indeed, DC101 inhibited tumor angiogenesis and growth, but at the same time it increased cancer invasiveness as well as the incidence, volume, and number of LN and liver metastases (Figure 9 and Supplemental Figure 7, A–C). Interestingly, when Sema3A treatment was combined with DC101, we observed a strong reduction of tumor invasiveness and metastasis formation compared with DC101-treated mice and controls (Figure 9, B–G).

In addition, whereas insulinomas treated with DC101 were highly hypoxic and displayed a less pericyte-covered, leakier, and poorly perfused vasculature, the combination of DC101 with Sema3A strongly reduced tumor hypoxia, increased blood vessel coverage, and restored the functionality of the tumor vasculature (Figure 10). Additionally, DC101 exerted a milder effect on the tumor vasculature than did sunitinib. In fact, although it strongly inhibited the blood vessel area, DC101 reduced the pericyte coverage of blood vessels less severely than sunitinib did (compare Figure 10, C–H, and Figure 4, A–F). Of note, in tumors treated with DC101, we observed a decreased number of $NG2^+$, PDGFR-β^+, and $desmin^+$ pericytes, but a significant increase of α-SMA^+ perivascular cells, compared with controls (Figure 10, D–H). These observations corroborate recent data showing that treatment of RIP-Tag2 mice with DC101 specifically increased the content of α-SMA^+ pericytes, but not perivascular cells identified by other markers (33).

Compared with the control, DC101 significantly impaired the perfusion and increased the permeability of tumor blood vessels, (Figure 10, I and J, and Supplemental Figure 8, A–D), which suggests that the DC101-induced rise of α-SMA^+ pericytes was not sufficient to maintain the function of blood vessels and indicates that the other pericyte subpopulations would indeed be necessary to fully normalize and improve the function of the tumor vasculature. Accordingly, simultaneous treatment with DC101 and Sema3A strongly increased all the subpopulation of pericytes ($NG2^+$, PDGFR-β^+, $desmin^+$, and α-SMA^+) and simultaneously improved the perfusion and reduced the vascular leakage, similar to Sema3A treatment alone (Figure 10, D–J, and Supplemental Figure 8, A–D). Together, these findings indicate that Sema3A is able to counteract the evasive resistance induced by the specific inhibition of VEGF signal pathways.

Discussion

Using 2 transgenic mouse models of spontaneous tumorigenesis, RIP-Tag2 and HPV16/E_2, we here demonstrate what we believe to be a novel role for Sema3A in overcoming the evasive resistance previously observed in preclinical mouse models upon angiogenesis inhibition (10, 11). When used as single therapeutic agent, Sema3A strongly inhibited tumor growth, similar to the effects of sunitinib and DC101; however, different from these latter drugs, Sema3A also impaired tumor invasion and dissemination to distal organs. Moreover, thanks to its vascular normalizing activity, Sema3A ameliorated blood vessel function, improved cancer tissue oxygenation, and lessened several hypoxia-regulated signaling pathways that support tumor progression and invasion. Consequently, Sema3A efficiently drove sunitinib- or DC101-treated tumors back from a prometastatic to a benign phenotype.

Recently, several reports on acquired resistance to antiangiogenic therapies highlighted the need to revisit the current therapies and

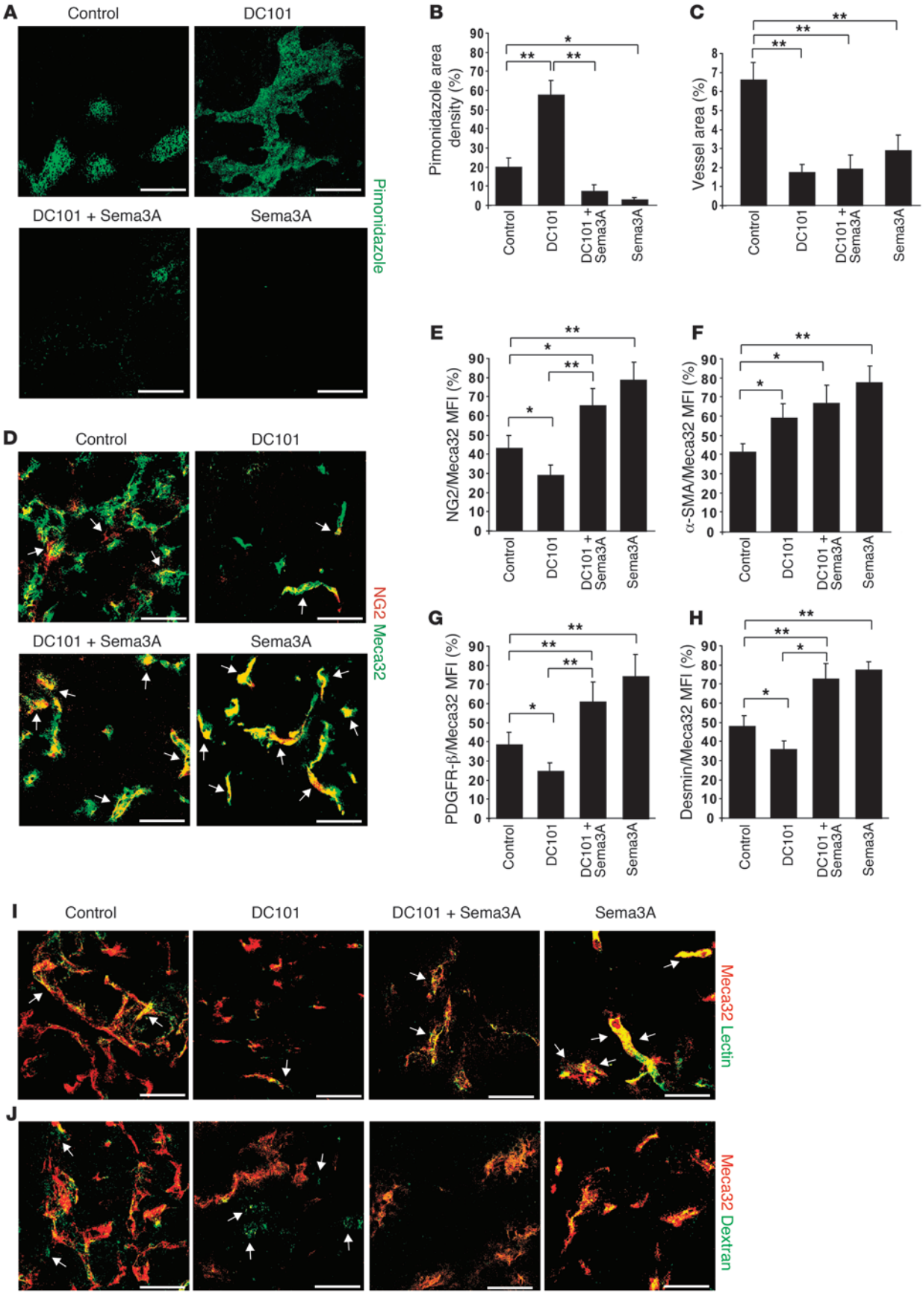
A
Control
DC101
DC101 + Sema3A
Sema3A
Pimonidazole
B
Pimonidazole area density (%)
Control
DC101
DC101 + Sema3A
Sema3A
C
Vessel area (%)
D
NG2 Meca32
E
NG2/Meca32 MFI (%)
F
α-SMA/Meca32 MFI (%)
G
PDGFR-β/Meca32 MFI (%)
H
Desmin/Meca32 MFI (%)
I
Meca32 Lectin
J
Meca32 Dextran

Figure 10
Sema3A impairs DC101-induced hypoxia and improves tumor blood vessel function. (**A**) Tumor hypoxia, assessed by pimonidazole adduct immunostaining (arrows) in tumors from mice treated as indicated for 4 weeks. (**B**) Quantification of hypoxic tumors, expressed as percent pimonidazole density area per tumor, per animal. Sema3A and DC101 combined decreased hypoxia 88% compared with DC101 alone; Sema3A decreased hypoxia 90% compared with controls. (**C**) Vessel density, as assessed by confocal microscopy of Meca32 immunostaining, was reduced 75%, 73%, and 50% by treatment with DC101, DC101 plus Sema3A, and Sema3A, respectively, compared with controls. (**D**–**H**) Pericyte coverage, as evaluated by confocal colocalization (arrows) of Meca32 with NG2 (**D** and **E**) or with α-SMA (**F**), PDGFR-β (**G**), or desmin (**H**) and expressed as percent colocalization of pericyte markers on tumor ECs. Combined Sema3A and DC101 enhanced pericyte coverage 56% (NG2), 59% (PDGFR-β), and 48% (desmin) compared with DC101. Sema3A increased pericyte coverage 45% (NG2), 47% (PDGFR-β), and 40% (desmin) compared with controls. DC101 increased α-SMA$^+$ pericyte coverage 46% versus controls. (**I**) Increased incidence of FITC-lectin–perfused vessels (arrows) in Sema3A-treated (alone or in combination with DC101) tumors compared with DC101-treated and control insulinomas. (**J**) Decreased FITC-dextran extravasation (arrows) in Sema3A-treated (alone or in combination with DC101) tumors compared with DC101-treated and control insulinomas. Results are from 5 fields per mouse (n = 8 per treatment group). *P < 0.05, **P < 0.01, unpaired Mann-Whitney U test. Scale bars: 50 μm.

investigate the possibility of combining tumor shrinkage (induced by cancer starvation from oxygen and nutrients) with blood vessel normalization to effectively counteract the metastatic dissemination of cancer cells, favored, for example, by a hypoxic microenvironment (34). Here, we showed that the combination of Sema3A with sunitinib synergistically enhanced RIP-Tag2 mouse survival and reduced HPV16/E_2 mouse tumor burden, finally inducing less invasive and less frequent metastatic cancers in both transgenic mouse models. Thus, administration of Sema3A in combination with sunitinib may represent an innovative and more efficient therapeutic strategy, thanks to the coupling of sunitinib's robust antitumorigenic and antiangiogenic activities (observed in several human tumors; refs. 35, 36) with Sema3A's pronormalizing, antiinvasive, and antimetastatic activities. The main mechanism by which Sema3A overcame the evasive resistance both to sunitinib and to DC101 was the ability of this repulsive guidance cue to restore tumor tissue oxygenation as a result of its powerful blood vessel normalizing activity. It is known that the pharmacological targeting of pericytes may disrupt the integrity of the tumor vasculature, thus enabling cancer cells to transit into the circulation system and metastasize (37). Therefore, our data suggest that the vascular normalizing effect of Sema3A could reduce the proinvasive effects of sunitinib by simultaneously inducing tumor tissue normoxia and blocking cancer cell extravasation.

It has been proposed that the duration of the vascular normalization window is critical to the achievement of long-lasting and successful therapeutic synergy between antiangiogenic and chemotherapeutic drugs (6, 18, 19, 38). Notably, all our different trials demonstrated that Sema3A, alone or in combination with sunitinib, significantly extended the normalization window of tumor blood vessels and improved the delivering efficiency of chemotherapeutic drugs to cancer tissues, by proportionally restraining the number of blood vessels and simultaneously favoring their coverage, maturation, and function. It is therefore conceivable to hypothesize new treatment strategies in which Sema3A could be combined with other clinically approved chemotherapeutic and/or antiangiogenic compounds.

The strong inhibition of HIF-1α protein expression we observed, due to the restoration of tumor tissue oxygenation upon combined treatment with Sema3A and sunitinib, highlights the crucial role played by Sema3A in overcoming the resistance to antiangiogenic therapies. Several HIF-1α inhibitors identified thus far strongly impair tumor progression in xenograft tumor models and are either in the early stages of clinical trials or FDA approved for anticancer therapy (3, 39). Notably, it has previously been shown that the combination of bevacizumab and irinotecan, a topoisomerase I inhibitor that also inhibits HIF-1α, induced clinical benefit in glioblastoma patients (40). By correlating the anti-invasive and antimetastatic effects of Sema3A on hypoxia-stressed cancers with the inhibition of expression of HIF-1α and its target genes, such as the TK receptor Met, our data further corroborate the main concept that combining HIF-1α inhibitors with antiangiogenic drugs can increase the therapeutic efficacy and avoid the described side effects (3).

In recent years, several mechanisms of intrinsic and acquired resistance to antiangiogenic agents have been described (14, 41). For instance, preclinical studies provided evidence of anti-VEGF drug evasion by activation of alternative pathways of angiogenesis and tumor progression (2). RIP-Tag2 mice have shown rapid adaptation to anti-VEGF agents, followed by tumor regrowth as a result of FGF signaling activation (4). An additional possibility could therefore be that activation of proangiogenic pathways, such as those triggered by FGFs, can be involved in developing sunitinib resistance in RIP-Tag2 mice and that the addition of Sema3A can inhibit the activation of these compensatory signal pathways. Interestingly, the data we obtained by combining Sema3A with DC101 further corroborated and strengthened the results obtained with sunitinib and demonstrated that by normalizing the vasculature and reducing tumor hypoxia, Sema3A overcame the evasive resistance induced by inhibition of both VEGF (via DC101) and multiple TK receptor–dependent signaling pathways (via sunitinib). Notably, our observation of an enhanced number of α-SMA$^+$ mural cells, paralleled by a simultaneous reduction of the other pericyte subpopulations (i.e., NG2$^+$, PDGFR-β$^+$, and desmin$^+$ cells), corroborates recent data showing that treatment of RIP-Tag2 mice with DC101 specifically increases the content of α-SMA$^+$ pericytes (33). As those authors suggested, DC101 is likely to induce a subpopulation of tumor blood vessels covered by α-SMA$^+$ pericytes deriving from co-opted blood vessels. One could hence speculate that the increased amount of tumor blood vessels surrounded by α-SMA$^+$ pericytes may be attributable to the milder effect that DC101 exerts on blood vessel perfusion and permeability compared with sunitinib. However, since we observed that DC101 significantly impaired perfusion and increased the permeability of tumor blood vessels compared with controls, such a DC101-induced rise in α-SMA$^+$ pericytes does not appear sufficient to support the reconstitution of physiologically functioning blood vessels. Therefore, the other pericyte subpopulations seem to be necessary to warrant the appearance of an efficiently normalized tumor vasculature. Accordingly, simultaneous treatment with DC101 and Sema3A, similar to what we observed with Sema3A alone, strongly increased all the pericyte subpopulations and simultaneously improved the perfusion and reduced the vascular leakage. These observations indicate that sunitinib and DC101 exert different effects on the tumor vasculature, suggesting

how these 2 drugs may induce evasive resistance to angiogenesis inhibition through different molecular mechanisms. Indeed, similar to sunitinib, DC101 triggered tumor hypoxia, but, differently from sunitinib, also co-opted blood vessels, a phenomenon that has previously been correlated with the development of acquired resistance to antiangiogenic therapies in RIP-Tag2 mice (4).

In this study, we showed that treating RIP-Tag2 tumors with sunitinib highly increased NF-κB expression. Since NF-κB activates HIF-1α and promotes EMT, cancer invasion, and tumor angiogenesis in several tumor types (25, 26, 42), our data suggest that NF-κB plays an important role in the development of evasive resistance in response to standard antiangiogenic therapies and that inhibition of NF-κB expression may represent a further mechanism by which Sema3A can overcome the side effects caused by angiogenesis inhibition. It has also been observed that during progression, tumors recruit proangiogenic myeloid cells that can contribute to the intrinsic resistance to antiangiogenic therapies (43). Of note, $Gr1^+MMP9^+$ cells, which increase the bioavailability of VEGF for its receptors (44), and tumor-associated macrophages (TAMs) expressing cathepsins B and S are critical promoters of tumor growth, angiogenesis, and invasion in RIP-Tag2 mice (45). Because NF-κB orchestrates the tissue inflammatory response induced by hypoxia, including leukocyte infiltration (25, 46, 47), it is conceivable that, by upregulating NF-κB expression, sunitinib could induce the recruitment and activation of neutrophils, TAMs, and other protumoral myeloid cells. Simultaneous administration of Sema3A together with sunitinib restored tumor tissue normoxia and reduced NF-κB, and could therefore inhibit the appearance of these inflammatory cell populations. Further studies are required to clarify the effect of Sema3A on bone marrow–derived proangiogenic cells during angiogenesis inhibition.

Inhibition of tumor angiogenesis by sunitinib strongly increased the expression and tyrosine phosphorylation of Met receptor in RIP-Tag2 tumors. Met and phospho-Met were present in cancer cells and, to a lesser extent, in vessels of untreated mice, highlighting the key role played by the Met receptor in tumor angiogenesis and progression (48–50). Notably, 1 month of sunitinib treatment strongly increased Met phosphorylation in tumor cells and not in ECs, suggestive of specific activation of the proinvasive HGF/Met pathway in cancer cells, but not in the tumor vasculature. The dramatic inhibition of Met expression and phosphorylation induced by Sema3A, alone or in combination with sunitinib, along with the substantial reduction of tumor spreading and metastatization indicated that HGF/Met signaling inhibition is an additional key mechanism by which Sema3A can overcome the evasive resistance to antiangiogenic therapies.

It is worth noting that treatment of tumor-bearing RIP-Tag2 mice with AVV8-Sema3A as a single agent reduced invasiveness and metastasis formation by increasing E-cadherin expression and inhibiting Met TK receptor activation in cancer cells compared with control insulinomas. Even though untreated tumors displayed a milder hypoxia than did sunitinib-treated insulinomas, 2 hypoxia-induced genes, CA9 and NF-κB, were significantly reduced in Sema3A-treated mice compared with controls. We speculate that Sema3A, by completely restoring tumor oxygenation and by inhibiting hypoxia-induced signal pathways in end-stage RIP-Tag2 tumors, may be responsible for the observed increase of E-cadherin levels, inhibition of Met activation, and consequent reduction of tumor invasion and metastatization. However, given the complexity of the tumor microenvironment (14, 41), complementary mechanisms may also mediate the effects of Sema3A on tumor angiogenesis and cancer progression. Further investigation is hence needed to clarify these aspects.

In conclusion, our studies indicate that Sema3A administration may represent a new therapeutic approach to inhibit angiogenesis, while promoting the maturation of the surviving vasculature and hence avoiding the commonly observed long-lasting tumor hypoxia that, if not hindered, can support the lethal dissemination of cancer cells throughout the body. This pharmacological strategy may help to better and safely harness the therapeutic potential of antiangiogenic drugs for the final benefit of oncologic patients.

Methods

Further information can be found in Supplemental Methods.

Transgenic tumor model. The RIP-Tag2 transgenic mouse model has been previously described (10, 13, 51). RIP-Tag2 mice were generated and maintained in the C57BL/6 background (Jackson Laboratory). From 12 weeks of age, all RIP-Tag2 mice received 50% sugar food (Harlan Teklad) and 5% sugar water to relieve hypoglycemia induced by the insulin-secreting tumors. Generation of K14-HPV16 transgenic mice (52) and E_2 treatment for cervical carcinogenesis has been previously reported (30, 31). Briefly, 1-month-old virgin female transgenic (heterozygous K14-HPV16) were anesthetized, and continuous-release pellets that deliver E_2 at 0.05-mg doses over 60 days (Innovative Research of America Inc.) were implanted s.c. in the dorsal back skin. Subsequent pellets were implanted at 3 and 5 months of age. The resulting HPV16/E_2 mice were maintained in the FVB/n background (The Jackson Laboratory). Mice were monitored throughout the experiments for complications caused by the dysplastic nature of their skin or by E_2 treatment.

Therapeutic treatments. Tumor- bearing RIP-Tag2 or HPV16/E_2 mice were treated for 4 weeks, from 12 until 16 weeks or from 5 until 6 months of age, respectively (regression trial). Different regression trials were designed: (a) 40 mg/kg/d sunitinib L-malate (Axon Medchem BV) was administered daily by oral gavage (n = 30); (b) 1 mg/mouse rat monoclonal function-blocking antibodies against VEGFR-2 (DC101), obtained in bulk by affinity purification from the supernatant of a hybridoma culture (DC101) (Translational Research Laboratory, Catalan Institute of Oncology), was administered twice weekly i.p. (n = 15), as previously reported (4); (c) 100 μl Sema3A was injected slowly through the abdominal aorta of RIP-Tag2 mice using a 30-gauge needle (Roboz Surgical Instrument) (n = 30), as previously described (13), or through the distal portion of the abdominal aorta just before its bifurcation into the 2 common iliac arteries of HPV16/E_2 mice (n = 12 per group) (see *In vivo AAV8 administration*); and (d) Sema3A-injected mice were treated daily by oral gavage with 40 mg/kg/d sunitinib L-malate or twice weekly with 1 mg/mouse DC101 (n = 15). Control mice were injected with LacZ (13) and treated with methylcellulose vehicle daily by oral gavage (n = 30) or with 1 mg/mouse purified rat IgG (Jackson Immunoresearch) i.p. (n = 15). For the survival trial, 12-week-old Rip-Tag2 mice were treated with 40 mg/kg/d sunitinib, Sema3A, combined Sema3A and sunitinib, or LacZ plus vehicle (n = 20 per group), and their survival was monitored over time.

In vivo AAV8 administration. AAV8-Sema3A was administered in RIP-Tag2 mice as previously described (13). For AAV8-LacZ or AAV8-Sema3A delivery in HPV16/E_2 mice, animals were anesthetized by 1.5% isoflurane anesthesia. The distal portion of the abdominal aorta just before its bifurcation into the 2 common iliac arteries was exposed following a displacement of intestine and urinary bladder and isolated from the surrounding fat tissue. 50 μl recombinant AAV8-Sema3A or AAV8-LacZ virus was injected slowly through the abdominal aorta, by means of a 31-gauge needle of an insulin syringe. After injection, homeostasis was performed. The abdomen was then closed layer-to-layer with 5-0 chromic gut sutures. Animals were subsequently mon-

itored and allowed to recover 1–2 hours after surgery. Postsurgical analgesia was achieved by buprenorphine (0.1 mg/kg s.c. every 12 hours for 1 day) and antibiotic prophylaxis with ampicillin (150 mg/kg s.c.).

Invasion index and metastasis analysis. Paraffin sections of pancreas, liver, and LN from each group of treatment were serially cut (10 μm) and rehydrated through 100% xylene and 100%, 95%, and 70% ethanol before immersion in 1× PBS. Sections were stained with H&E as previously described (10). Tissues were visualized with a BX-60 microscope (Olympus) equipped with a color Qicam Fast 1394-digital CCD camera (12 bits; QImaging Corp.). The invasion index of tumors was determined using 5 H&E-stained sections per animal. Based on gross morphological and detailed histopathological characteristics, tumor islets were subdivided into insulinomas with well-defined margins and frequent fibrous capsules (IT), carcinomas with focal regions of invasion (IC1), or fully invasive carcinomas (IC2) (10). The presence or absence of tumor cell dissemination was first evaluated by H&E staining and confirmed by rabbit anti-SV40 T-antigen (sc-20800, 1:50; Santa Cruz) or HPV16-E7 (250629, 1:100; Abbiotec) Abs and by immunofluorescence, according to previously described protocols. LN and liver metastasis incidence in RIP-Tag2 mice and lung and liver metastasis incidence in HPV16/E_2 transgenic mice was evaluated by scoring for presence or absence in each animal using 10 sections per animal. The number of liver metastases was measured as SV40 T-antigen or HPV16-E7 protein-positive regions in 10 images per mouse per treatment group. To quantify the metastatic volume, we used ImageJ software to compare the metastatic mass with a spheroid. In each image, we drew a line corresponding to the width (w) of the metastatic region and a line corresponding to the length (l), then calculated the LN metastatic volume as $0.52 \times w^2 \times l$, as for a spheroid.

Tumor hypoxia analysis. The amount of tumor hypoxia was determined 2 hours after injection of 60 mg/kg pimonidazole hydrochloride (HP2-100 Hypoxyprobe Kit-Plus; Natural Pharmacia International Inc.) into RIP-Tag2 mice (13). The formation of pimonidazole adducts was detected by immunostaining with Hypoxyprobe-1-Mab1 FITC Ab according to the manufacturer's instructions. Immunofluorescence images were captured and analyzed using a Leica TCS SP2 AOBS confocal laser-scanning microscope (Leica Microsystems) and then evaluated by Image-ProPlus 6.2 software (Media Cybernetics). Quantification was done by analyzing at least 5 sections and 5 fields per tumor.

Tumor vessel perfusion and vascular permeability. To detect tumor vessel perfusion and vascular permeability, mice were injected i.v. with 0.05 mg FITC-labeled tomato lectin (Lycopersicon esculentum; Vector Laboratories) or 0.05 mg 70-kDa FITC-conjugated dextran (Molecular Probes). After 2 minutes, the animals were euthanized, and the heart was perfused with saline solution followed by 2% PFA. Lectin and dextran distribution was visualized by fluorescent confocal microscopy z-sectioning that allowed for 3D reconstruction of the vascular network.

Confocal microscopy quantifications. To quantify pericyte coverage (NG2, α-SMA, PDGFR-β, or desmin, shown by red channels) in each image, we drew a region of interest (ROI) close to each blood vessel (Meca32, shown by green channels) and then quantified the MFI of red and green channels using the Leica Confocal Software Histogram Quantification Tool. We then calculated the ratio between red and green channel MFI; values are expressed as percentage of red-green costaining. A similar procedure was followed to quantify vascular perfusion by FITC-labeled lectin. Blood vessel permeability was analyzed by measuring the area of dextran extravasation. To determine the expression levels of E-cadherin (green channel), vimentin (red channel), total Met, and phospho-Met (red channel) in each analyzed image, we considered 5 random ROIs of the same size. Then we measured the ratio between the red or green channel and the blue (DAPI) channel MFI; data are presented as percent positive cells relative to total cell number.

Measurement of in vivo tumor bioavailability of doxorubicin. A group of RIP-Tag2 mice, previously treated for 4 weeks with LacZ plus vehicle (control) or with Sema3A, sunitinib, or Sema3A and sunitinib combined, was injected with 10 mg/kg doxorubicin hydrochloride (Sigma-Aldrich) via the lateral tail vein 4 hours before sacrifice. Pancreatic tumors and kidneys as controls were collected from each mouse and weighed. Samples were resuspended in a lysis buffer (0.25 M sucrose, 5 mM TrisHCl pH 7.6, 1 mM $MgSO_4$, 1 mM $CaCl_2$) and homogenized in an ice-cold Potter homogenizer. 200 μl of each homogenate was placed into a new microcentrifuge tube, and 100 μl 10% Triton X-100, 200 μl water, and 1.5 ml acidified isopropanol was added. The mixture was vortexed and kept at –20°C overnight. The next day, samples were warmed to room temperature ad centrifuged at 15,000 *g* for 20 minutes. Doxorubicin was quantified by spectrophotometric analysis (λ ex, 470 nm; λ em, 590 nm) using the Synergy HT (BioTek) plate reader. These values were compared with a standard curve of known amounts of doxorubicin and normalized based on the weight of the each organ and on the fluorescence emission of the control tissue, calculated as the fluorescence/weight ratio of the tumor divided by the fluorescence/weight ratio of the kidney. Data are mean ± SD of triplicate aliquots from tumor homogenates expressed as μ equivalents/g tissue of doxorubicin.

Statistics. All values are expressed as mean ± SD. For all statistical analyses, a 2-tailed, unpaired Mann-Whitney U test was used. Statistical analysis for the survival trial was performed using the log-rank test. A P value less than 0.05 was considered significant.

Study approval. All animal procedures were approved by the Ethical Commission of the University of Torino and by the Italian Ministry of Health in compliance with the international laws and policies.

Acknowledgments

We thank Marta Paez-Ribes for helping to evaluate tumor invasiveness and metastasis formation and Doug Hanahan for discussion and insightful suggestions. This work was supported by Associazione Italiana per la Ricerca sul Cancro (AIRC) investigator grants (5837 to E. Giraudo, 9211 to G. Serini, and 10133 to F. Bussolino); by AIRC 2010 Special Program in Molecular Clinical Oncology 5% Project no. 9970 (to E. Giraudo and F. Bussolino); by Regione Piemonte Ricerca Sanitaria Finalizzata 2007, 2008, and 2008 bis (to E. Giraudo, G. Serini, and F. Bussolino); by Ricerca industriale e sviluppo precompetitivo 2006 grants PRESTO and SPLASERBA (to F. Bussolino); by Associazione Augusto per la Vita (to G. Serini); by Compagnia di San Paolo — Neuroscience Program Multicentre Projects (to G. Serini); by Ministero della Salute Programma di Ricerca Finalizzata 2006 and Programma Straordinario di Ricerca Oncologica 2006 (to E. Giraudo and F. Bussolino); by Converging Technologies grant PHOENICS (to E. Giraudo and F. Bussolino); by Fondazione Guido Berlucchi (to E. Giraudo and G. Serini); by Fondazione Cassa di Risparmio Torino (CRT) (to E. Giraudo and F. Bussolino); by Fondazione Piemontese per la Ricerca sul Cancro-ONLUS (Intramural Grant 5% 2008) (to E. Giraudo and G. Serini); and by Telethon Italy (to G. Serini). F. Maione was supported by fellowship "26 fellowship — FIRC" granted by Fondazione Italiana per la Ricerca sul Cancro (FIRC).

Received for publication May 12, 2011, and accepted in revised form February 22, 2012.

Address correspondence to: Enrico Giraudo, Laboratory of Transgenic Mouse Models, IRCC, and Department of Oncological Sciences, University of Torino School of Medicine, Strada Provinciale 142, Km 3.95, I-10060 Candiolo, Turin, Italy. Phone: 39.011.9933505; Fax: 39.011.9933524; E-mail: enrico.giraudo@ircc.it.

1. Folkman J. Angiogenesis. *Annu Rev Med*. 2006; 57:1–18.
2. Duda DG, Batchelor TT, Willett CG, Jain RK. VEGF-targeted cancer therapy strategies: current progress, hurdles and future prospects. *Trends Mol Med*. 2007;13(6):223–230.
3. Rapisarda A, Melillo G. Role of the hypoxic tumor microenvironment in the resistance to anti-angiogenic therapies. *Drug Resist Updat*. 2009;12(3):74–80.
4. Casanovas O, Hicklin DJ, Bergers G, Hanahan D. Drug resistance by evasion of antiangiogenic targeting of VEGF signaling in late-stage pancreatic islet tumors. *Cancer Cell*. 2005;8(4):299–309.
5. Baluk P, Hashizume H, McDonald DM. Cellular abnormalities of blood vessels as targets in cancer. *Curr Opin Genet Dev*. 2005;15(1):102–111.
6. Jain RK. Normalization of tumor vasculature: an emerging concept in antiangiogenic therapy. *Science*. 2005;307(5706):58–62.
7. Semenza GL. Hypoxia and cancer. *Cancer Metastasis Rev*. 2007;26(2):223–224.
8. Sabbah M, et al. Molecular signature and therapeutic perspective of the epithelial–to–mesenchymal transitions in epithelial cancers. *Drug Resist Updat*. 2008;11(4–5):123–151.
9. Pennacchietti S, Michieli P, Galluzzo M, Mazzone M, Giordano S, Comoglio PM. Hypoxia promotes invasive growth by transcriptional activation of the met protooncogene. *Cancer Cell*. 2003;3(4):347–361.
10. Paez-Ribes M, et al. Antiangiogenic therapy elicits malignant progression of tumors to increased local invasion and distant metastasis. *Cancer Cell*. 2009;15(3):220–231.
11. Ebos JM, Lee CR, Cruz-Munoz W, Bjarnason GA, Christensen JG, Kerbel RS. Accelerated metastasis after short-term treatment with a potent inhibitor of tumor angiogenesis. *Cancer Cell*. 2009;15(3):232–239.
12. Galluzzo M, Pennacchietti S, Rosano S, Comoglio PM, Michieli P. Prevention of hypoxia by myoglobin expression in human tumor cells promotes differentiation and inhibits metastasis. *J Clin Invest*. 2009;119(4):865–875.
13. Maione F, et al. Semaphorin 3A is an endogenous angiogenesis inhibitor that blocks tumor growth and normalizes tumor vasculature in transgenic mouse models. *J Clin Invest*. 2009;119(11):3356–3372.
14. Bergers G, Hanahan D. Modes of resistance to anti-angiogenic therapy. *Nat Rev Cancer*. 2008; 8(8):592–603.
15. Christensen JG. A preclinical review of sunitinib, a multitargeted receptor tyrosine kinase inhibitor with anti-angiogenic and antitumour activities. *Ann Oncol*. 2007;18 suppl 10:x3–x10.
16. Casazza A, et al. Systemic and targeted delivery of semaphorin 3A inhibits tumor angiogenesis and progression in mouse tumor models. *Arterioscler Thromb Vasc Biol*. 2011;31(4):741–749.
17. Sathornsumetee S, et al. Tumor angiogenic and hypoxic profiles predict radiographic response and survival in malignant astrocytoma patients treated with bevacizumab and irinotecan. *J Clin Oncol*. 2008;26(2):271–278.
18. Winkler F, et al. Kinetics of vascular normalization by VEGFR2 blockade governs brain tumor response to radiation: role of oxygenation, angiopoietin-1, and matrix metalloproteinases. *Cancer Cell*. 2004;6(6):553–563.
19. Goel S, et al. Normalization of the vasculature for treatment of cancer and other diseases. *Physiol Rev*. 2011;91(3):1071–1121.
20. Bergers G, Song S, Meyer-Morse N, Bergsland E, Hanahan D. Benefits of targeting both pericytes and endothelial cells in the tumor vasculature with kinase inhibitors. *J Clin Invest*. 2003;111(9):1287–1295.
21. Yilmaz M, Christofori G. EMT, the cytoskeleton, and cancer cell invasion. *Cancer Metastasis Rev*. 2009;28(1–2):15–33.
22. Perl AK, Wilgenbus P, Dahl U, Semb H, Christofori G. A causal role for E-cadherin in the transition from adenoma to carcinoma. *Nature*. 1998; 392(6672):190–193.
23. McConkey DJ, et al. Role of epithelial–to–mesenchymal transition (EMT) in drug sensitivity and metastasis in bladder cancer. *Cancer Metastasis Rev*. 2009;28(3–4):335–344.
24. Min C, Eddy SF, Sherr DH, Sonenshein GE. NF-kappaB and epithelial to mesenchymal transition of cancer. *J Cell Biochem*. 2008;104(3):733–744.
25. Sarkar FH, Li Y, Wang Z, Kong D. NF-kappaB signaling pathway and its therapeutic implications in human diseases. *Int Rev Immunol*. 2008; 27(5):293–319.
26. van Uden P, Kenneth NS, Rocha S. Regulation of hypoxia-inducible factor-1alpha by NF-kappaB. *Biochem J*. 2008;412(3):477–484.
27. Cummins EP, et al. Prolyl hydroxylase-1 negatively regulates IkappaB kinase-beta, giving insight into hypoxia-induced NFkappaB activity. *Proc Natl Acad Sci U S A*. 2006;103(48):18154–18159.
28. Culver C, Sundqvist A, Mudie S, Melvin A, Xirodimas D, Rocha S. Mechanism of hypoxia-induced NF-kappaB. *Mol Cell Biol*. 2010;30(20):4901–4921.
29. Smith-McCune K, Zhu YH, Hanahan D, Arbeit J. Cross-species comparison of angiogenesis during the premalignant stages of squamous carcinogenesis in the human cervix and K14-HPV16 transgenic mice. *Cancer Res*. 1997;57(7):1294–1300.
30. Giraudo E, Inoue M, Hanahan D. An aminobisphosphonate targets MMP-9-expressing macrophages and angiogenesis to impair cervical carcinogenesis. *J Clin Invest*. 2004;114(5):623–633.
31. Arbeit JM, Howley PM, Hanahan D. Chronic estrogen-induced cervical and vaginal squamous carcinogenesis in human papillomavirus type 16 transgenic mice. *Proc Natl Acad Sci U S A*. 1996; 93(7):2930–2935.
32. Seeber LM, et al. The role of hypoxia inducible factor-1alpha in gynecological cancer. *Crit Rev Oncol Hematol*. 2011;78(3):173–184.
33. Franco M, Paez-Ribes M, Cortez E, Casanovas O, Pietras K. Use of a mouse model of pancreatic neuroendocrine tumors to find pericyte biomarkers of resistance to anti-angiogenic therapy. *Horm Metab Res*. 2011;43(12):884–889.
34. Carmeliet P, Jain RK. Principles and mechanisms of vessel normalization for cancer and other angiogenic diseases. *Nat Rev Drug Discov*. 2011;10(6):417–427.
35. Goodman VL, et al. Approval summary: sunitinib for the treatment of imatinib refractory or intolerant gastrointestinal stromal tumors and advanced renal cell carcinoma. *Clin Cancer Res*. 2007;13(5):1367–1373.
36. Raymond E, et al. Sunitinib malate for the treatment of pancreatic neuroendocrine tumors. *N Engl J Med*. 2011;364(6):501–513.
37. Xian X, et al. Pericytes limit tumor cell metastasis. *J Clin Invest*. 2006;116(3):642–651.
38. Sorensen AG, et al. A "vascular normalization index" as potential mechanistic biomarker to predict survival after a single dose of cediranib in recurrent glioblastoma patients. *Cancer Res*. 2009; 69(13):5296–5300.
39. Rapisarda A, et al. Schedule-dependent inhibition of hypoxia-inducible factor-1alpha protein accumulation, angiogenesis, and tumor growth by topotecan in U251-HRE glioblastoma xenografts. *Cancer Res*. 2004;64(19):6845–6848.
40. Vredenburgh JJ, et al. Bevacizumab plus irinotecan in recurrent glioblastoma multiforme. *J Clin Oncol*. 2007;25(30):4722–4729.
41. Carmeliet P, Jain RK. Molecular mechanisms and clinical applications of angiogenesis. *Nature*. 2011;473(7347):298–307.
42. Nam SY, et al. A hypoxia-dependent upregulation of hypoxia-inducible factor-1 by nuclear factor-kappaB promotes gastric tumour growth and angiogenesis. *Br J Cancer*. 2011;104(1):166–174.
43. Shojaei F, et al. Bv8 regulates myeloid-cell-dependent tumour angiogenesis. *Nature*. 2007; 450(7171):825–831.
44. Nozawa H, Chiu C, Hanahan D. Infiltrating neutrophils mediate the initial angiogenic switch in a mouse model of multistage carcinogenesis. *Proc Natl Acad Sci U S A*. 2006;103(33):12493–12498.
45. Gocheva V, et al. IL-4 induces cathepsin protease activity in tumor-associated macrophages to promote cancer growth and invasion. *Genes Dev*. 2010; 24(3):241–255.
46. Fitzpatrick SF, et al. An intact canonical NF-kappaB pathway is required for inflammatory gene expression in response to hypoxia. *J Immunol*. 2011; 186(2):1091–1096.
47. Porta C, et al. Cellular and molecular pathways linking inflammation and cancer. *Immunobiology*. 2009;214(9–10):761–777.
48. Christensen J, Anderes K. Beyond VEGF: targeting tumor growth and angiogenesis via alternative mechanisms. *Adv Exp Med Biol*. 2008;610:43–53.
49. Abounader R, Laterra J. Scatter factor/hepatocyte growth factor in brain tumor growth and angiogenesis. *Neuro Oncol*. 2005;7(4):436–451.
50. Bussolino F, et al. Hepatocyte growth factor is a potent angiogenic factor which stimulates endothelial cell motility and growth. *J Cell Biol*. 1992;119(3):629–641.
51. Hanahan D. Heritable formation of pancreatic beta-cell tumours in transgenic mice expressing recombinant insulin/simian virus 40 oncogenes. *Nature*. 1985;315(6015):115–122.
52. Coussens LM, Hanahan D, Arbeit JM. Genetic predisposition and parameters of malignant progression in K14-HPV16 transgenic mice. *Am J Pathol*. 1996;149(6):1899–1917.